MULTI-BEAM RECEIVING ANTENNA FOR THE BAND 3-30 MHz

A thesis submitted for the
degree of Doctor of Philosophy
in the Faculty of Engineering,
University of London

by

António Francisco Ferreira dos Santos

September 1970

Department of Electrical Engineering
Imperial College of Science and Technology
London

ACKNOWLEDGEMENTS

The author is grateful to Mr. H. Page and Prof. J. Brown for their suggestions and guidance in the research.

The author is indebted to Calouste Gulbenkian Foundation, Lisbon, for financial support during the realisation of the present work.

He also wishes to thank Signals Research and Development Establishment, Ministry of Technology, for their interest in and support for the project and Mr. W.A. Gurnhill for his cooperation in the construction of the experimental model.

ABSTRACT

A proposal for a new multi-beam antenna to operate in the high-frequency band (3-30 MHz) is presented. The characteristics of this antenna are determined and its performance compared with that of the Luneberg-lens.

The proposed antenna is a circular array of radially-arranged Beverage elements and consequently part of the thesis is devoted to the study of the Beverage antenna (horizontal wire at low height above ground). The problem of calculating the near field of the Beverage antenna and its propagation constant is analysed. A new theoretical approach is used and it is shown that the structure can support two modes that may propagate simultaneously. Numerical techniques for solving the equation for the propagation constant are given. The theoretical results are compared with measurements made on a small-scale model.

Ways of improving the performance of the Beverage antenna are proposed and the possibility of extending its application to frequencies above 30 MHz is briefly discussed.

CONTENTS

1. INTRODUCTION

This thesis deals with an investigation aimed at developing a directional antenna for the high-frequency band (3-30MHz) to be used for receiving signals propagating via the ionosphere. The antenna was required to be capable of receiving simultaneously a number of transmissions which could arrive from any azimuthal direction. It must, therefore, provide a number of independent outputs associated with beams pointing in different directions.

One antenna system that satisfies this requirement is a group or "farm" of rhombics. Each rhombic covers a frequency band of only about 2:1, but two or more such rhombics can be mounted one inside the other to cover a wider band. To cater for a range of directions, however, it is necessary to use a large number of such units, so that the total site area required is very large. An alternative solution is the multi-beam antenna which differs from the farm of rhombics in that any element of the multi-beam antenna is used to form several beams. Consequently, for the same

directivity, the multi-beam antenna can be designed to occupy a much smaller area.

In section 1.1. we examine briefly the main characteristics of several multi-beam antennas that have been reported in the literature in the past ten years. In section 1.2. we describe a new multi-beam system, the radial travelling-wave antenna, which appears to have some advantage over the existing ones; it combines structural simplicity with good overall performance.

The radial travelling-wave antenna consists essentially of an array of radially-arranged horizontal wires (Beverage elements) with appropriate phase compensation. The study of the characteristics of the array elements is the object of chapters 2 and 3. Chapter 2 deals with the theory of electromagnetic-wave propagation along an infinitely long horizontal wire and, in particular, with the calculation of the propagation constant. Chapter 3 deals with the determination of the radiation characteristics of the Beverage elements.

Chapter 4 is devoted to the study of the radial travelling-wave antenna as an array, and to the computation of its performance. The dependence of the directional properties of the antenna on its geometrical configuration is analysed with a view to determining a "nearly-optimum" system.

1.1. Survey of Existing H.F. Multi-Beam Antennas

1.1.1. The Medusa System

The Medusa System[1],[2] (multiple-direction universally steerable antenna) shown schematically in Fig.1.1, is an array of randomly spaced wide-band vertical elements spread over an approximately circular area. To form a beam pointing in a particular direction the outputs of the different elements are brought approximately into phase for a plane wave coming from that direction.

Multiple beams are obtained by dividing the output of each element into a number of channels (see Fig.1.1) corresponding to different phasing networks. Wide-band amplifiers are inserted between the antennas and the power dividers in order to avoid a degradation of the signal-to-noise ratio. The phase correction of each antenna is selected in a 4-way switch controled by a digital computer. Thus, only four different phase shifts are used. This greatly simplifies the design of the phase-shift network, but means that phase errors of up to $\pm 45^{\circ}$ may occur. It is shown in ref.2 that the power gain of the system is very little affected by these errors; the effect on side-lobe level is not mentioned but some degradation in performance is to be expected.

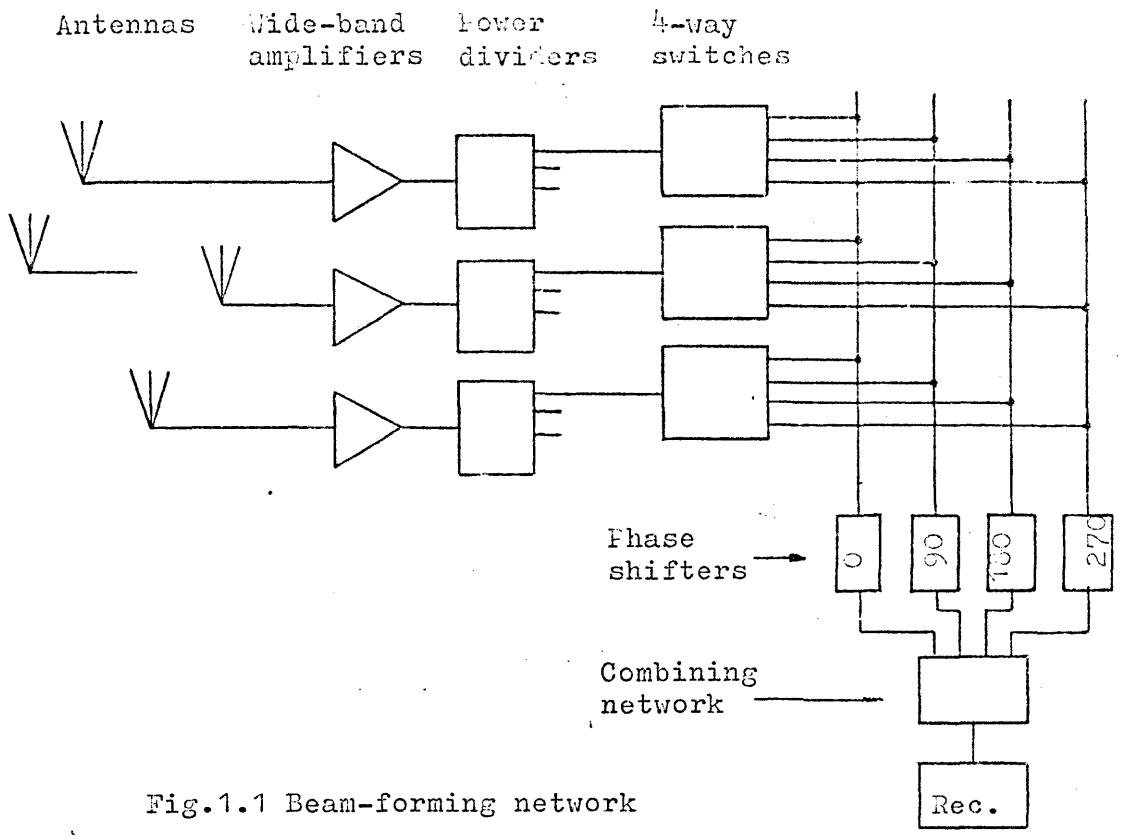

Fig.1.1 Beam-forming network of the Medusa System

The medusa system can be continuously steered in both azimuth and elevation and its performance appears to be better than that of a rhombic. The side-lobe level depends on the number of aerials per unit area and on the size of the system. However, in the case of the system described in ref. 2 (300m diameter, 48 elements) side lobes as high as -6dB can occur. The azimuthal beamwidth to the 3dB points varies from 5 to 2 degrees within the frequency band 5-25MHz.

1.1.2. The Wire-Grid Lens Antenna

The wire-grid lens antenna [3],[4] is a two-dimensional Luneberg lens* terminating in a cylindrical horn as shown schematically in Fig. 1.2. The antenna derives its directivity in the

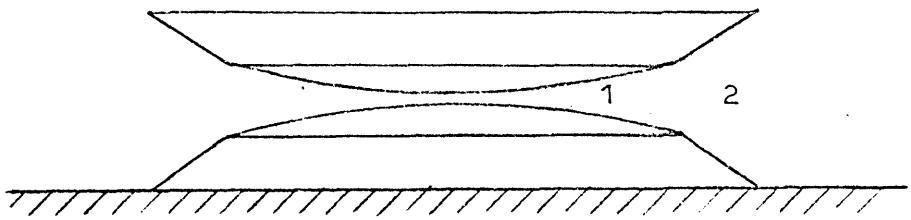

1-lens 2-horn

Fig. 1.2.Cross section of the lens antenna

horizontal plane from the focusing effect of the Luneberg lens. This is illustrated qualitatively in Fig.1.3; the wave front of an incoming plane wave bends progressively as it travels inside the lens so that its energy is focused on a point in the lens periphery

---

* The two-dimensional Luneberg lens is a circularly-symmetrical lens whose refractive index (n) varies with distance to the centre of the lens (r) according to the formula $n(r)=\sqrt{2-(r/a)^2}$ where a is the lens radius [5].

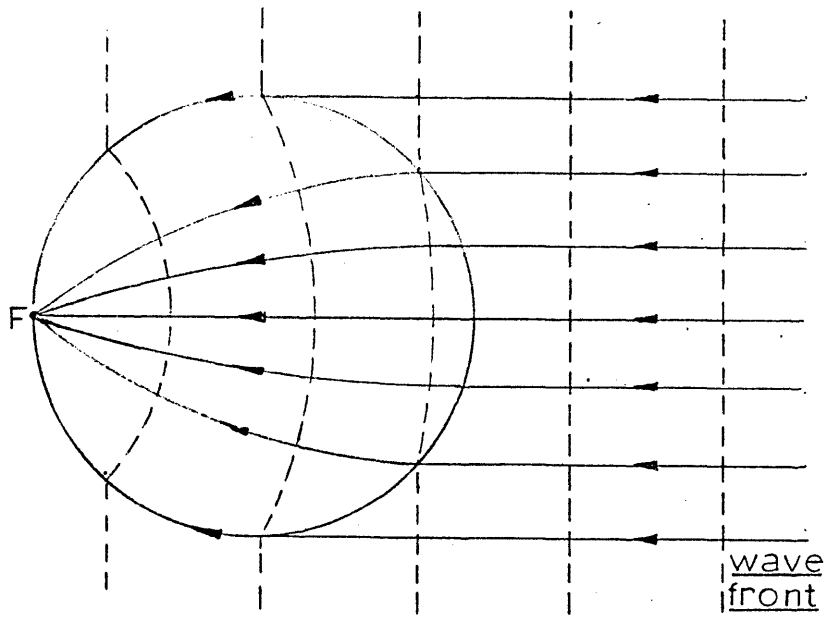

Fig. 1.3. Focusing effect of the Luneberg lens

opposite to the direction of arrival.

The Luneberg lens was originally proposed as an optical lens [5]; the equivalent h.f. lens[3] consists of two wire-grids whose spacing and mesh size are varied to achieve the required value of the refractive index. In order to obtain multiple beams a number of feeds are placed round the lens at equal intervals. These feeds are short travelling-wave antennas coupled to the modes that propagate inside the lens. The horizontal directivity of this type of feed increases with frequency, hence reducing the effective size of the lens aperture at the higher frequencies. This is advantageous because it makes the beamwidth less dependent on frequency.

Typically the antenna system occupies a circular area 320m in diameter. The beamwidth varies from 25 degrees at 3MHz to 8 degrees at 30MHz and the peak side-lobe level from -7dB at 3MHz to -15dB at 30MHz.

1.1.3. Circular Array of Vertical Antennas

The two multi-beam antennas referred to in the preceding sections have performances comparable to that of a "farm" of rhombics but both are very complex systems and consequently very costly.

A much simpler system is described in refs.6 and 7. This is a phase-compensated circular array of omnidirectional elements. To obtain a multi-beam antenna each element of the array is connected to a number of phasing networks through a power divider (Fig. 1.4) as in the Medusa system. The signals are brought into phase by means of delay lines and combined in hybrid transformers. Since these are wide-band components the same phasing network covers the whole frequency band of the system.

The antenna system described in ref. 7 occupies a circular area 150m in diameter and covers the frequency range 1.5-10MHz. Each beam is synthesised from the elements that lie in an angular sector of 120 degrees centred on the direction of the beam. The side-lobe ratio is rather low, varying between 6 and 9 dB, and cannot be improved except by using directive elements. This pos-

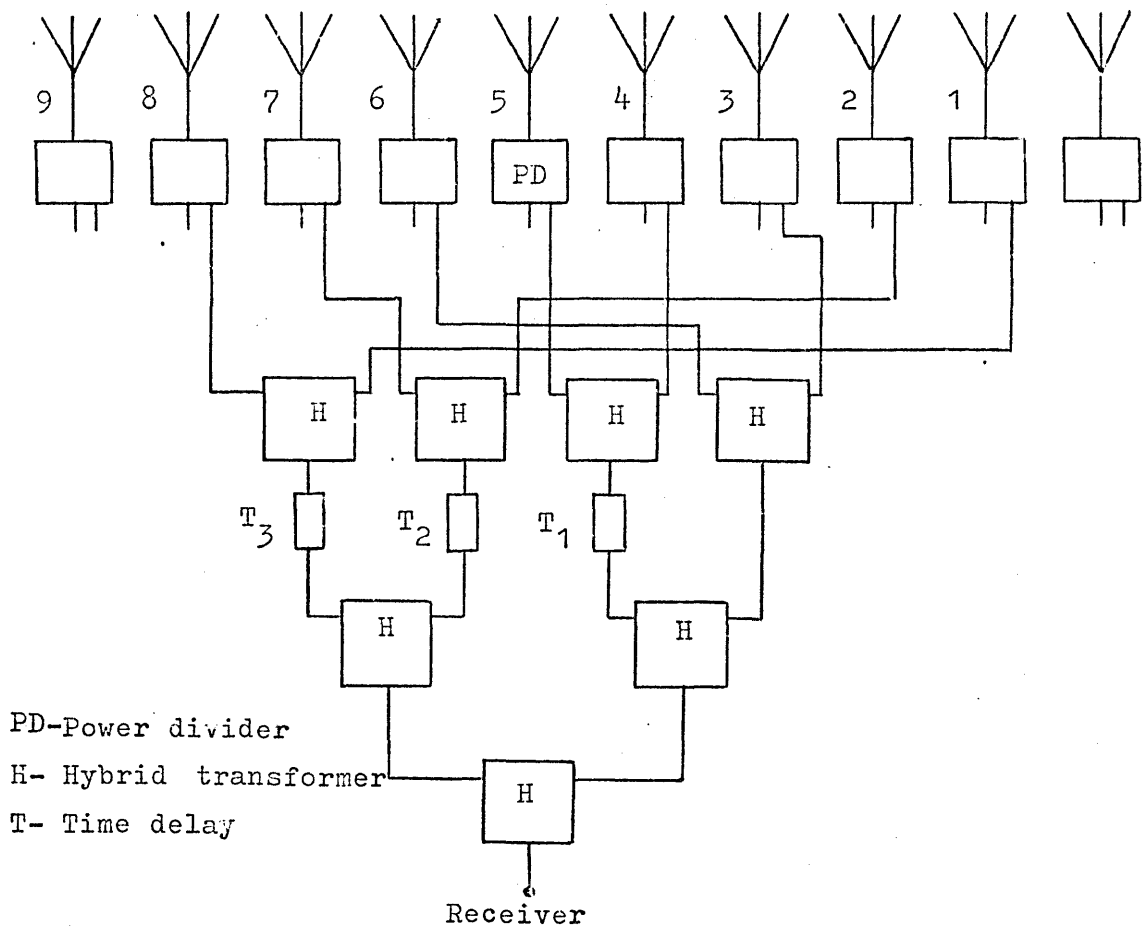

Fig. 1.4. Beam-forming network

sibility is discussed further in the next section.

1.2. The Radial Travelling-Wave Antenna

In the preceding sections we examined briefly the main characteristics of three types of multi-beam h.f. antennas that have been reported in the literature. The Medusa system and the

wire-grid lens antenna have performances comparable to or better than the "farm" of rhombics but are highly complex systems. The circular array of vertical antennas described in 1.1.3. is a simple system but exhibits poor side-lobe characteristics.

Thus, we set out to investigate whether a multi-beam antenna combining relative constructional simplicity with good overall performance could be devised.

A first idea to be considered was a radial arrangement of travelling-wave antennas, consisting of a number of Beverage antennas occupying a circular area and extending along the whole diameter of the circle. By using both ends as feed points each antenna would cover two opposite azimuthal sectors. The Beverage antenna (long horizontal wire at low height above ground and terminated in a matched load) was chosen because of its constructional simplicity and very broad band characteristics. However it was found that, for the same beamwidth, the arrangement of diametral travelling-wave antennas would require four times the area of the wire-grid lens antenna.

A second idea to be considered was a circular array of radial Beverage antennas with phase compensation. It is known that low side lobes can be obtained from circular arrays providing the elements are directive and their excitation appropriately tapered[8]. Hence, in respect of side-lobe performance a circular

array of Beverage elements does not have the limitations of the system described in section 1.1.3. In addition, the broad-band characteristics of the Beverage element permit covering the whole h.f. band (3-30MHz) .

The phase-compensated circular array of Beverage elements ,a sector of which is represented in Fig.1.5, will be hereafter referred to as the radial travelling-wave antenna. Multiple

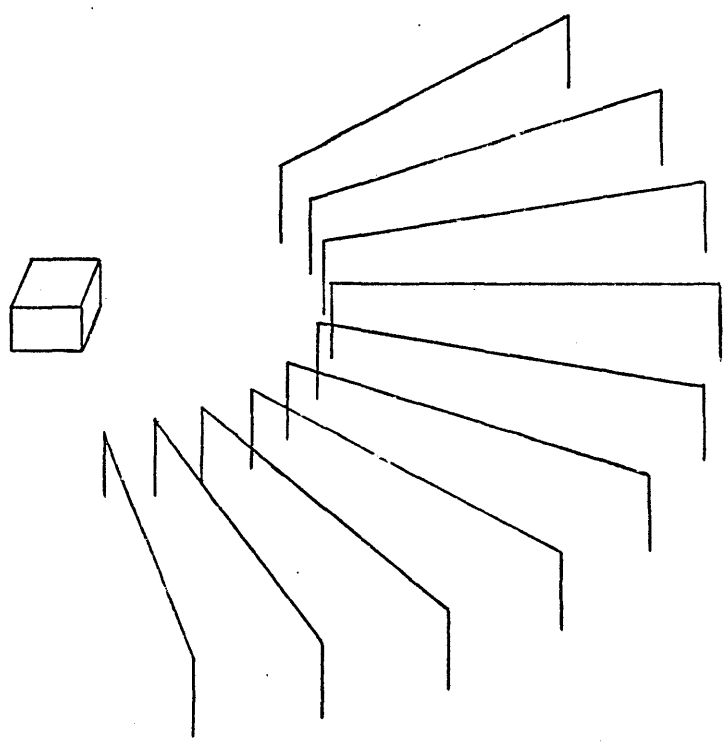

Fig. 1.5. Arrangement of elements in the radial travelling-wave antenna

beams are obtained from this system by means of a beam-forming network similar to that of Fig. 1.4 but, to prevent the degradation of the signal-to-noise ratio due to internal noise in the system, wide-band amplifiers must be inserted between the array elements and the power dividers.

The performance of the radial travelling-wave antenna is determined mainly by the two parameters that define its geometrical configuration—diameter and ratio of element length to radius of the system— and by the angular sector corresponding to the elements used to form a beam*. The study of the general characteristics of the system as functions of these parameters (chapter 4.) shows that there is no set of values that optimises all the radiation characteristics, and thus a compromise choice has to be made.

The dimensions proposed are:

diameter of the occupied circle	300m
element length	90m
element height	1m
element spacing	5^{o}

---

* This will be called the active sector.

Active sector:	3-6 MHz	155°
	6-18 MHz	75°
	18-30 MHz	35°

The active sector must decrease with frequency because it is directly linked to the beamwidth of the elements.

The beamwidth of a radial travelling-wave antenna with the above mentioned dimensions, varies from 30 degrees at 3MHz to 9 degrees at 30MHz. The side-lobe level varies between -14 and -18 dB.

In comparison to the wire-grid lens antenna which occupies a similar area, the proposed system has broader beams (+4° at 3MHz, +1° at 30MHz) but a lower side-lobe level (-8dB at 3MHz, -2dB at 30MHz). It appears, therefore, that the radial travelling-wave antenna is both simple and technically satisfactory.

References

1. D.Morris and G. Mitchell "A multiple-direction universally steerable aerial system for h.f. operation", Proc. I.E.E. Vol.106B p.555,1959.

2. D.Morris, G. Mitchell, E.May, C.Hughes and D.Dalgleish "An experimental multiple-direction universally steerable aerial system for h.f. reception", Proc. I.E.E. Vol. 110 p. 1569,

September 1963.

3. R.Tanner and M.Andreasen "A wire-grid lens antenna of wide application" Parts I and II, I.R.E. Trans. on Antennas and Propagation Vol.AP-10 pp. 408-429, July 1962.

4. E. Jones, R.Tanner, E.Sharp, M.Andreasen and F.Harris "Performance of the wire-grid lens h.f. antenna" I.R.E. Trans. on Antennas and Propagation Vol. AP-15 p. 744, November 1967.

5. A.Z.Fradin "Microwave antennas" Pergamon Press 1961,section VI.7.

6. I.D.Longstaff and D.E.Davies "A wideband circular array for h.f. communications" Radio and Electronic Engineer Vol.35 p. 321 June 1968.

7. J.T.Starbuck "A multiple-beam high-frequency receiving aerial system" Radio and Electronic Engineer Vol.36 p. 229 April 1969.

8. P.W.James "Polar patterns of phase-corrected circular arrays" Proc. I.E.E. ,Vol 112 p.1839, October 1965.

2. ELECTROMAGNETIC-WAVE PROPAGATION ALONG A HORIZONTAL WIRE ABOVE GROUND

2.1. Introduction

The problem of calculating the field of a wave propagating along a horizontal wire above ground was first investigated by J.R.Carson[1] and F.Pollaczek[2] in 1926. Pollaczek calculated the field of a uniform line source above ground, at low frequency, whereas Carson attempted the solution of the wave equation assuming a velocity of propagation near to the velocity of light in the air. Carson formulated the problem in terms of the distributed-parameter theory and derived an expression for the distributed series impedance of the equivalent transmission line. His analysis is based on three simplifying assumptions: (a) the two-dimensional wave equation can be substituted by Laplace's equation in the dielectric medium; (b) the displacement current in the ground is negligible compared with the conduction current; (c) the change in the paralleladmittance per unit length due to the finite conductivity of

the ground is negligible. The first assumption is valid in most cases of practical interest but the validity of the second and third assumptions is restricted to low frequencies.

In 1933 W.H.Wise[3] extended the validity of Carson's analysis removing assumption (b). He obtained an expression for the series impedance by integrating the field of a horizontal dipole along an infinite length of wire.

In 1955 H.Kikuchi[4] first derived an expression for the parallel admittance per unit length and showed that the attenuation constant does not increase indefinitely with frequency but exhibits a maximum and tends to zero as the frequency tends to infinity. Kikuchi solved the wave equation for the interface boundary conditions but, to obtain an expression for the propagation constant, neglected the transverse wave number in the dielectric medium which amounts to substituting Laplace's equation for the wave equation in that medium.

In this chapter we deal with the same boundary-value problem without resorting to transmission-line theory. The equation for the transverse wave number is derived by imposing the condition that the tangential electric field be zero on the axis of the wire. The electromagnetic field is expressed in terms of a Hertz vector potential which simplifies the problem formulation and yields expressions formally similar to those obtained for a

horizontal electric dipole.

It is shown that there are two possible solutions of the wave equation: a proper solution which vanishes at infinity and an improper solution which violates the radiation condition. Above the wire, the improper mode has the character of a superposition of outgoing waves and the proper mode that of a superposition of incoming waves. By analogy with what happens in two-dimensional leaky-wave structures[5] it is suggested that, in the case of the improper mode, there is radiation loss in addition to dissipation in the ground.

The solution presented in Kikuchi's paper purports to correspond to the proper mode. However, in sections 2.5 and 2.6 it is shown that, in some cases, his approximate method for evaluating the inverse Fourier transform of the field (quasi-T.E.M. approximation) may not be valid for the proper mode but is always accurate for the improper mode.

The equation for the transverse wave number h_1 is solved numerically without making any assumptions about the order of magnitude of h_1; this makes it possible to do a comparative study of the two propagating modes and of the accuracy of the quasi-T.E.M. approximation.

In section 2.7. the values of the propagation constant

for the proper and improper modes are compared with those measured on a small-scale model. The experimental results show that when the launching device is a generator located between the horizontal wire and the ground, as in the case of the Beverage antenna, it is the improper mode that is excited.

2.2. Problem Formulation

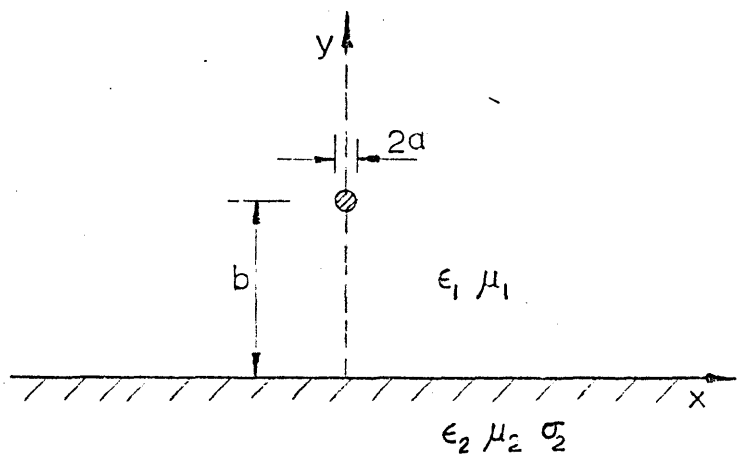

Fig. 2.1

Consider an infinitely long horizontal wire placed at height b above imperfectly conducting ground as shown schematically in Fig.1. In order to simplify the computations it will be assumed that the radius of the wire is small compared with the

height ($b/a \gg 1$). In this case the transverse currents are negligible in comparison with the longitudinal currents and the field can be expressed in terms of an electric Hertz vector ($\bar{\Pi}$) with no x component, in the same way as for a horizontal electric dipole radiating in presence of the earth (See ref. 6 section 1.4). Furthermore, the current distribution on the wire can be assumed to be uniform.

The fields $\bar{E}$ and $\bar{H}$ are obtained from the Hertz vector through the equations[7]*

$$\begin{aligned} \bar{E} &= \bar{\nabla}\times\bar{\nabla}\times\bar{\Pi} \\ \bar{H} &= (\sigma+j\omega\epsilon)\,\nabla\times\bar{\Pi} \end{aligned} \qquad (1)$$

Taking into consideration that $\Pi_x=0$ we write

$$\bar{\Pi} = \Psi\,\bar{a}_y+\Phi\,\bar{a}_z \qquad (2)$$

For a z dependence of the form $\exp\{-\gamma z\}$ the potentials Φ and Ψ satisfy the two-dimensionsl eigen-value equation

$$\left(\frac{\partial^2}{\partial x^2}+\frac{\partial^2}{\partial y^2}+h_m^2\right)\begin{Bmatrix}\Phi_m\\ \Psi_m\end{Bmatrix} = 0 \qquad (3)$$

in the two homogeneous regions. In this equation m denotes the medium; subscript 1 denotes the upper or dielectric medium (free

---

* A time dependence of the form $\exp\{j\omega t\}$ is assumed.

space) and subscript 2 the lower or conducting medium (the ground). We have:

$$h_m^2 = k_m^2 + \gamma^2 \tag{4}$$

$$k_m^2 = \omega^2 \epsilon_m \mu_m \left(1 - j\frac{\sigma_m}{\omega \epsilon_m}\right)$$

$$= \begin{cases} \omega^2 \epsilon_o \mu_o & \text{For the dielectric medium.} \\ \omega^2 \epsilon_o \mu_o n^2 & \text{For the conducting medium.} \end{cases} \tag{5}$$

where n is the complex refractive index of the ground

$$n = \sqrt{\frac{\epsilon_2}{\epsilon_o} - j\frac{\sigma_2}{\omega \epsilon_o}} \tag{6}$$

To solve the interface boundary-value problem it is convenient to split the function Φ_1 in two terms

$$\Phi_1 = \Phi_{10} + \Phi_{11}$$

where Φ_{10} arises from the currents in the wire and Φ_{11} from the currents in the ground. For thin wires ($b/a \gg 1$) we can consider Φ_{10} to be due to a line source at x =0, y =b in which case Φ_{10} satisfies the non-homogeneous differential equation (7)

$$\left(\frac{\partial^2}{\partial x^2} + \frac{\partial^2}{\partial y^2} + h_1^2\right)\Phi_{10} = j\frac{I}{\omega \epsilon_o}\delta(x)\delta(y-b) \tag{7}$$

in the dielectric medium. The remaining functions Φ_{11}, Φ_2, Ψ_1

and Ψ_2 satisfy the homogeneous equation (3) everywhere. Φ_{10} can be regarded as a wave incident on the interface, Φ_{11} and Ψ_1 as reflected waves and Φ_2 and Ψ_2 as waves transmitted into the conducting medium.

Φ_{10} is obtained by solving eq. 7; the remaining functions are related to Φ_{10} through the conditions of continuity of the tangential components of $\bar{E}$ and $\bar{H}$ at the interface. From (1) the following relations are obtained:

$$\Phi_1 = n^2 \Phi_2 \qquad (8.a)$$

$$\Psi_1 = n^2 \Psi_2 \qquad (8.b)$$

$$\frac{\partial \Phi_1}{\partial y} = n^2 \frac{\partial \Phi_2}{\partial y} \qquad (8.c)$$

$$\frac{\partial \Psi_1}{\partial y} - \gamma \bar{\Phi}_1 = \frac{\partial \Psi_2}{\partial y} - \gamma \bar{\Phi}_2 \qquad (8.d)$$

which are valid for y = 0. To complete the formulation of the problem, the boundary condition at infinity is required. However the formulation of this condition raises some difficulties which are discussed in the next section.

2.3. Integral Representation of the Field

The solutions of eq.3 can be expressed in the form of

Fourier integrals* as follows

$$\Phi_m = \int_C F_m(s)\, e^{-j(u_m|y| + sx)}\, ds \qquad (9.a)$$

$$\Psi_m = \int_C P_m(s)\, e^{-j(u_m|y| + sx)}\, ds \qquad (9.b)$$

provided that

$$u_m = \sqrt{h_m^2 - s^2} \qquad (10)$$

The integration contour C and the branch of u must be chosen so that the integrals (9) converge; in addition, if it is assumed that the field is excited by a source located between the wire and the ground, eqs. 9 must represent outgoing waves at infinity in the +y and -y directions. These two conditions are satisfied if

$$\text{Real}\{u\} \geqslant 0 \qquad (11.a)$$

$$\text{Im}\{u\} \lesseqgtr 0 \qquad (11.b)$$

on the contour C. In problems involving the solution of the wave equation in two or three dimensions a contour of integration can be found on which the above relations hold simultaneously (See

---

* The solution of eq. 7 can be expressed in the same form with y substituted by y-b (See Appendix 1.).

for example ref.8). However, eq.3 differs from the wave equation in that, whereas the wave number k has a non-positive imaginary part, in the dielectric medium h_1 has a positive imaginary part. In fact, writing $\gamma = \alpha + j\beta$ $(\alpha,\beta>0)$, $h_1 = h_r + jh_i$ $(h_r \geq 0)$ and substituting in (4) we obtain

$$h_r h_i = \alpha\beta$$

from which it follows that $h_i \geq 0$. This in turn implies that, if we take C to be the real axis, the argument of u_1^2 lies in the interval $(0, \pi)$ and thus

$$0 < \arg\{u_1\} < \pi/2 \quad \text{i.e.} \quad u_1 \to j|s| \quad \text{as} \quad |s| \to \infty$$

or

$$-\pi < \arg\{u_1\} < -\pi/2 \quad \text{i.e.} \quad u_1 \to -j|s| \quad \text{as} \quad |s| \to \infty$$

depending on which branch of u_1 is chosen. In order to ensure the convergence of the integrals in (9) we must choose the branch of u_1 corresponding to the latter relation in which case we have

$$\text{Real}\{u_1\} < 0 \qquad (12.a)$$

$$\text{Im}\{u_1\} < 0 \qquad (12.b)$$

on the contour C. Relation (12.a) signifies that, in the region above the wire, the field is represented by a superposition of incoming waves. If we let y tend to $+\infty$ the integrals (9) vanish because of (12.b), i.e. choosing the real axis for the contour C leads to a proper mode. This is the case considered by Kikuchi.

However a contour can be found that satisfies relation

11.a and leads to a converging integral representation. To this end, we define the proper branch of u_1 by relation 11.a and examine its behaviour in the complex s plane. By making the following substitutions in eq. 10

$$u = u_r + ju_i \ , \ s = s_r + js_i \ , \ h_1 = h_r + jh_i$$

we obtain

$$\begin{aligned} u_r^2 - u_i^2 &= h_r^2 - h_i^2 - s_r^2 + s_i^2 \\ u_r u_i &= h_r h_i - s_r s_i \end{aligned} \qquad (13)$$

The second of these equations shows that if $s_r s_i > h_r h_i$ we have $u_i < 0$ for $u_r > 0$. Consider now the contour C_i represented in Fig.2.2. On the parts of the contour that run along the branch cut $u_r = 0$,

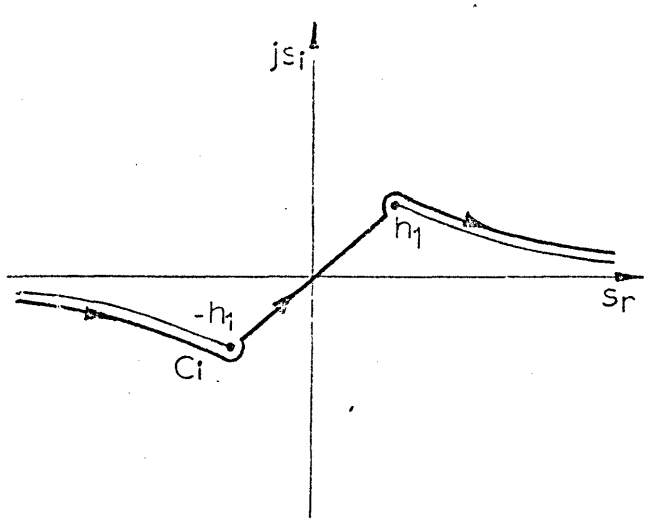

Fig. 2.2

we have $s_r s_i > h_r h_i$. Letting s_r approach infinity we obtain from (13)

$$u_i \to -|s_r| \quad \text{and} \quad u \to -j|s_r|$$

which ensures that the integrals (9) exist. On the part of the contour running from $-h_1$ to h_1 we have $u_i \geqslant 0$ since $s_r s_i < h_r h_i$. This implies that if y tends to infinity the integrals (9) diverge which in turn means that the corresponding solution is an improper one.

A greater insight into the question of convergence of the integral representation of the potentials Φ and Ψ can be gained by making the conformal transformation

$$s = h_1 \sin \varphi \tag{14}$$

which maps the two sheets of the Riemann surface into the area bounded by the lines AA' and CC' in Fig.2.3. The lines AA' , BB' and CC' are the mappings of the branch cuts $u_r = 0$*. Writing

$$u_1 = h_1 \cos \varphi \tag{15}$$

the sheet of the Riemann surface defined by $u_r > 0$ is mapped into the strip bounded by AA' and BB'; the second sheet ($u_r < 0$) is mapped into the strip BB' , CC'*. Thus, the conformal transformation

---

* By writing $\varphi = \xi + j\lambda$ the equation of these lines is found to be $\tan \xi \tanh \lambda = -h_r/h_i$.

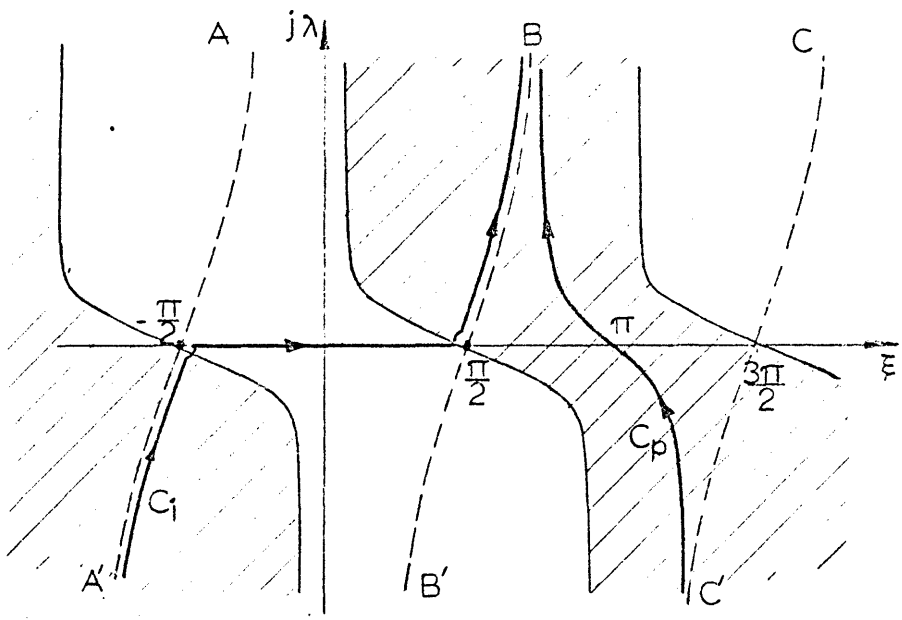

Fig. 2.3

(15) enables us to represent, in the same plane, the contours corresponding to the two possible solutions of eqs. 3 : C_i* refers to the improper mode and C_p to the proper mode. The fact that C_p remains entirely within the shaded area, where $u_i<0$, and part of C_i runs outside it, illustrates our previous remarks about the character of the solutions corresponding to the two contours.

Thus far we have only considered the convergence of the

---

* The same symbol is used for the contour C_i in the s and φ planes.

integral representation of the potentials in the upper medium. We now show that both C_i and C_p lead to converging integrals in the lower medium.

Writing $u_2=u_r+ju_i$, $h_2=h_r+jh_i$* and $s=s_r+js_i$, we obtain from (10)

$$u_r u_i = h_r h_i - s_r s_i$$

On the integration contour $s_r s_i \geqslant 0$. Taking into account that $h_r h_i < 0$ because of the term $-j\omega\mu\sigma$ in k_2^2 (See eq.5), we conclude that $u_r u_i < 0$ i.e. for the branch of u_2 defined by $u_r \geqslant 0$ we have $u_i \leqslant 0$ which ensures the convergence of the integral representation of the field in the conducting medium. Fig.2.4 shows

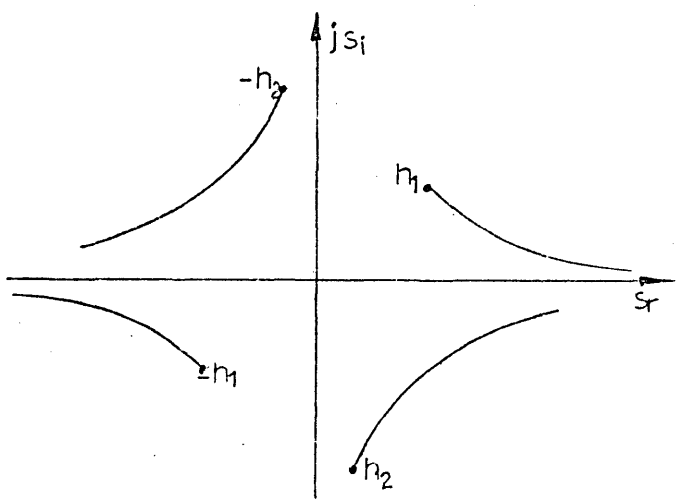

Fig. 2.4

---

* The omission of the subscript 2 should not lead to confusion with u_1 and h_1.

the relative position of all the branch points and branch cuts in the s plane.

2.4. Solution of the Boundary-Value Problem

As indicated in the preceding section the proper and improper modes differ only in the choice of the integration contour and of the branch of u_1. This permits carrying out the analysis in such a way that it is valid for both modes.

Firstly we substitute in eqs. 8 the Fourier integrals (9) for the functions Φ_{11} , Φ_2 , Ψ_1 and Ψ_2 ,together with the expression of Φ_{10} ($\Phi_1 = \Phi_{10} + \Phi_{11}$) derived in Appendix 1

$$\Phi_{10} = - \frac{I}{4\pi\omega\epsilon_o}\int_c \frac{\exp\{-ju_1|y-b|\}}{u_1}\, ds \qquad (16)$$

to obtain the following equations for the transforms

$$F_{11}+F_{10} = n^2 F_2 \qquad (17.a)$$

$$P_1 = n^2 P_2 \qquad (17.b)$$

$$u_1(F_{11}-F_{10}) = -n^2 u_2 F_2 \qquad (17.c)$$

$$u_1 P_1 - j\gamma(F_{11}+F_{10}) = -u_2 P_2 - j\gamma F_2 \qquad (17.d)$$

where

$$F_{10} = - \frac{I}{4\pi\omega\epsilon_o} \cdot \frac{e^{-ju_1 b}}{u_1} \qquad (18)$$

From (17.a) and (17.c) it follows that

$$F_{11} = -F_{10} - \frac{2A}{\pi (u_1+u_2)} e^{-ju_1 b} \qquad (19)$$

in which A is a constant given by

$$A = \frac{I}{4\omega\epsilon_o} \qquad (20)$$

Substituting (17.a) , (17.b) and (19) in (17.d) and solving for P_1 we obtain

$$P_1 = -j \frac{2\gamma A}{\pi} \cdot \frac{n^2-1}{(n^2u_1+u_2)(u_2+u_1)} e^{-ju_1 b}$$

which, by using the relation

$$n^2-1 = (k_2^2-k_1^2)/k_o^2 = (u_2^2-u_1^2)/k_o^2$$

simplifies to*

$$P_1 = -j \frac{2\gamma A}{\pi k_o^2} \cdot \frac{u_2-u_1}{n^2u_1+u_2} e^{-ju_1 b} \qquad (21)$$

From (9) ,(16) , (19) , A.5 (Appendix 1) and (21) we can now write the expressions for the potential functions Φ_1 and Ψ_1

---

*

Expressions (19) and (21) are analogous to those obtained for a horizontal electric dipole radiating in presence of the earth (See ref. 6 sections 2.22 and 2.33).

$$A^{-1}\Phi_1 = -\left[H_o^{(2)}(h_1R_1)-H_o^{(2)}(h_1R_2)\right] - \frac{2}{\pi}\int_{C_i} M(s)e^{-j\theta(s)}ds \qquad (22.a)$$

$$A^{-1}\Psi_1 = -j\,\frac{2\gamma}{\pi k_o^2}\int_{C_i} N(s)e^{-j\theta(s)}ds \qquad (22.b)$$

for the improper mode *. In these expressions

$$\theta(s) = u_1(y+b)+sx \qquad (23)$$

$$M(s) = \frac{1}{u_1+u_2} \qquad N(s) = \frac{u_2-u_1}{n^2u_1+u_2} \qquad (24)$$

$$R_1 = x^2+(y-b)^2 \qquad R_2 = x^2+(y+b)^2 \qquad (24)$$

The functions Φ_2 and Ψ_2 can be obtained in a similar way but are not needed in the subsequent analysis.

The equation for the transverse wave number is derived by imposing the condition that the axial component of the electric field be zero on the surface of the wire. But, since we have assumed a uniform current density on the wire and neglected the transverse currents, that condition can be exactly satisfied at only one point. For the same reasons E_x is zero only on the symmetry plane x=0. However, for thin wires ($b/a \gg 1$) the functions

---

* To obtain the corresponding formulae for the proper mode substitute C_i by C_p and $-H_o^{(2)}(\ \ )$ by $H_o^{(1)}(\ \ )$.

Φ_1 and Ψ_1 are approximately constant on the surface of the wire, as can be seen from (22), and the resulting error for h_1 is negligible.

From (1) and(22) the dispersion equation for the improper mode is found to be

$$H_o^{(2)}(h_1 a) - H_o^{(2)}(2h_1 b) + \frac{2}{\pi}\int_{C_i}\left(M - \frac{\gamma^2 u_1}{k_o^2 h_1^2} N\right)e^{-2ju_1 b}\,ds = 0 \qquad (26)$$

Similarly, for the proper mode we have

$$-H_o^{(1)}(h_1 a) + H_o^{(1)}(2h_1 b) + \frac{2}{\pi}\int_{C_p}\left(M - \frac{\gamma^2 u_1}{k_o^2 h_1^2} N\right)e^{-2ju_1 b}\,ds = 0 \qquad (27)$$

It should be borne in mind that in (26) $\text{Real}\{u_1\} \geq 0$ whereas in (27) $\text{Real}\{u_1\} \leq 0$.

2.5. Methods for Solving the Dispersion Equation

Before we deal with methods for solving the dispersion equations 26 and 27 it is useful to examine the behaviour of the function N(s) in the **s** plane. In fact N(s) exhibits a pair of first order poles which, as will be shown below, may affect significantly the value of this function on the contour C_p.

2.5.1. The Poles of N(s)

These poles occur for the values of s that satisfy the equation:

$$n^2 u_1 + u_2 = 0 \qquad (28)$$

Multiplying by $n^2 u_1 - u_2$ and using the relation

$$u_1^2 = u_2^2 - (n^2-1)k_o^2$$

we obtain

$$u_2 = \frac{n^2 k_o}{\sqrt{n^2+1}} \qquad (29)$$

In accordance with what has been said in section 2.3 we must choose the branch of the square root for which Real $\{u_2\} > 0$ i.e. the one that approaches n for very large values of this quantity. From (28) and (29) it follows that

$$u_1 = - \frac{k_o}{\sqrt{n^2+1}} \qquad (30)$$

i.e. $-\pi < \arg\{u_1\} < -\pi/2$ which signifies that the poles lie in the sheet of Riemann surface corresponding to the contour C_p. From (15) and (30) we obtain

$$\cos\varphi = - \frac{k_o}{h_1\sqrt{n^2+1}} \qquad (31)$$

The position of the poles in the φ plane can vary substantially

depending on the relative values of h_1 and $k_o/\sqrt{n^2+1}$. Fig. 2.5 illustrates a possible configuration. It is apparent from (31)

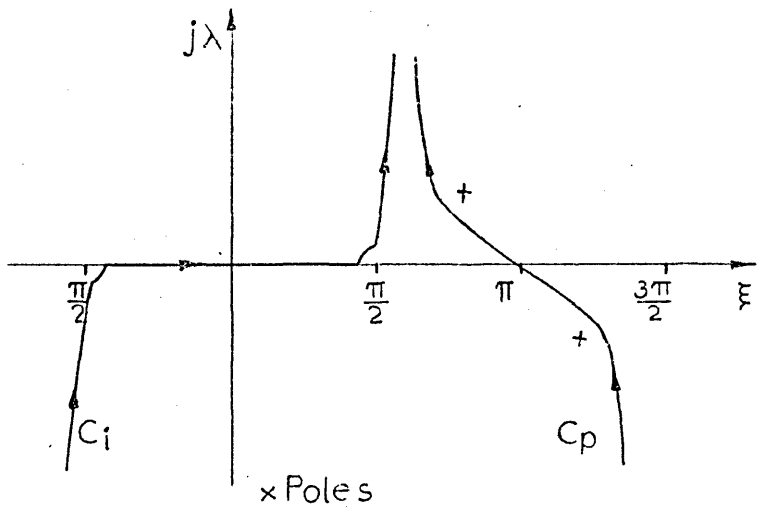

Fig. 2.5

that, for some values of the parameters of the system, the poles may be located close to the contour C_p and consequently some care is required when evaluating the integral (22.b) along C_p.

2.5.2. The Quasi-T.E.M. Approach

It is clear that eqs. 26 and 27 are not susceptible to exact solution by formal analysis because both u_1 and u_2 are functions of the eigen-value h_1^2. However if $2h_1 b \ll 1$ (quasi-T.E.M. mode) an approximate formula for h_1^2 can be easily derived and the

evaluation of the Fourier integrals greatly simplified.

Consider an integral of the general form

$$G = \int_C g(u_1) e^{-ju_1 d} ds \quad (*) \tag{32}$$

If $2h_1 b \ll 1$, which is true in most pratical cases, the exponent in the integrand of (32) is approximately equal to unity for values of s less than or of the order of h_1. This suggests the possibility of simplifying the integral by neglecting h_1 in u_1 i.e. putting

$$u_1 \simeq -js \tag{33}$$

which leads to

$$G = 2 \int_0^\infty g(-js) e^{-sd} ds \tag{34}$$

This is the method followed by Kikuchi[4]. It is similar to the quasi-static approximation used to calculate the near field of a dipole in presence of the earth[10][11] and corresponds to substituting Laplace's equation for eq.3 in the dielectric medium.

Approximation (34) makes the integral (32) independent of h_1^2 and yields the same result for the proper and improper modes. However, this approximation is not valid if the function

---

* Note that $u_2 = \sqrt{h_2^2 - s^2} = \sqrt{(n^2-1)k_o^2 + u_1^2}$

$g(u_1)$ varies rapidly in the range $|s| \ll |h_1|$. But this is precisely what may happen in the case of the proper mode since g may have a pair of poles in the vicinity of the origin. This point appears to have been overlooked by Kikuchi. It will be discussed further in section 2.6.

Turning to the solution of the dispersion equation we note that, if $2h_1 b \ll 1$, we have[12]

$$H_o^2(h_1 a) - H_o^{(2)}(2h_1 b) \simeq j \frac{2}{\pi} \ln \frac{2b}{a}$$

$$\simeq -H_o^{(1)}(h_1 a) + H_o^{(1)}(2h_1 b)$$

and eqs. 26 and 27 reduce to

$$j \ln \frac{2b}{a} + 2G_1 + 2jG_2\left(1 - \frac{k_o^2}{h_1^2}\right) = 0 \qquad (35)$$

where

$$G_1 = \int_0^\infty \frac{e^{-2bs}}{-js+u_2}\, ds \qquad (36.a)$$

$$G_2 = \frac{1}{k_o^2} \int_0^\infty s \frac{u_2+js}{-jn^2 s+u_2} e^{-2bs} ds \qquad (36.b)$$

Solving (35) for h_1^2 yields

$$h_1^2 = \frac{k_o^2 G_2}{\frac{1}{2}\ln \frac{2b}{a} - jG_1 + G_2} \qquad (37)$$

The quantities G_1 and G_2 given by (36) can be easily evaluated on the digital computer by means of the Gauss-Laguerre quadrature formula.(13)

2.5.3. Solution by Iterative Method

In order to compare the values of the propagation constant for the proper and improper modes and to assess the accuracy of formula (37) it is required to solve eqs. 26 and 27 without resorting to simplifying assumptions. This can be done by using an iterative technique such as Newton's method(14) providing some suitable means for evaluating the integrals (32) is found*.

This type of integral is not tractable by the methods of the infinitesimal calculus and, because the quantity $2h_1 b$ is normally much less than unity, an asymptotic expansion by the method of steepest descents is useless. A numerical integration along the contours C_i and C_p could be used but a more elegant and efficient technique is the numerical integration along the steepest descent path(15).

Consider the integral

---

* It is to be noted that the Hankel functions are represented by integrals of the form (32). However for $H_o^{(2)}(h_1 a)$ we can use the approximate formula(12) $H_o^{(2)}(h_1 a) \simeq 1 + j\frac{2}{\pi}[\ln(h_1 a/2) + \gamma]$ where γ is Euler's constant. For $H_o^{(1)}(h_1 a)$ the sign of the imaginary part is reversed.

$$G = \int_{C_i} g(u_1) e^{-ju_1 d}\, ds \qquad (32')$$

First we make the change of variable (14) and deform the contour C_i to transform it into a path of steepest descent*. Then by making the following change of variable

$$t = -j\sqrt{2jh_1 d}\, \sin\frac{\varphi}{2}$$

(32') is transformed into an integral along the real axis in the t plane (See Appendix 2)

$$G = 4h_1 e^{-jh_1 d} \int_0^\infty \frac{g_1(h_1 \cos\varphi)\cos\varphi}{\sqrt{2jh_1 d + t^2}}\, e^{-t^2}\, dt \qquad (38)$$

where

$$\cos\varphi = 1 - jt^2/h_1 d$$

A similar expression for the proper mode is given in Appendix 2.

Integral (38) is in a convenient form for numerical evaluation but the infinite interval must be truncated so that a quadrature formula for a finite interval may be used. In fact

---

* If the integral G refers to the proper mode and $g(u_1)$ contains N(s) it is necessary to check whether contributions from the poles have to be added.

there exists an integration formula (Gauss-Hermite [13]) for an integral of the type (38) but the number of points for which the weighting coefficients have been calculated is not sufficient for an acceptable accuracy to be attained. The truncation of the infinite interval at x=5 is normally accurate enough since $\exp\{-25\}$ is of the order of 10^{-11}. As for the particular integration formula to be used, Simpson's rule with interval halving, to ensure that the desired accuracy is reached, is a satisfactory choice.

We can now consider the solution of the dispersion equation. Eqs. 26 and 27 may be written in the general form

$$F(\lambda)=0 \qquad (39)$$

where $\lambda = h_1^2$. Newton's method requires the calculation of the derivative of $F(\lambda)$ which is impracticable because of the complexity of this function. This difficulty can be overcome by using the false-position algorithm[14] (regula falsi) which is a modification of Newton's method based on substituting the derivatives by the corresponding finite-difference quotients. Denoting by λ_n the value of λ used in the n^{th} iteration we have

$$\lambda_{n+1} = \lambda_n - \frac{(\lambda_n - \lambda_{n-1}) \cdot F(\lambda_n)}{F(\lambda_n) - F(\lambda_{n-1})} \qquad (40)$$

To initiate the process two distinct approximations to the root of (39) λ_o and λ_1 are required. These can be obtained from the value given by (37). The iterative process is stopped

when the ratio $(\lambda_{n+1} - \lambda_n)/\lambda_{n+1}$ falls below the required accuracy.

2.6. Numerical Results. Conclusions.

To test the accuracy of formula 37 and verify our conclusions about the validity of the quasi-T.E.M. approach in the case of the proper mode, we have computed the propagation constant by the two methods described in the preceding sections. The results for the attenuation constant are given in Fig. 2.6. and refer to the following parameters:

Height = 1m

Wire radius = 0.0025 m

Dielectric constant of the ground = 15

Conductivity of the ground = 0.01 S/m

Examination of Fig. 2.2 shows that the results obtained by the quasi-T.E.M approach are very close to those obtained for the improper mode but differ substantially from those corresponding to the proper mode over a wide range of frequencies. This confirms our remark that the presence of a pair of poles in the vicinity of the contour C_p may invalidate the assumption that substituting -js for u_1 does not alter significantly the value of the function N(s). A comparison between the phase velocity for the

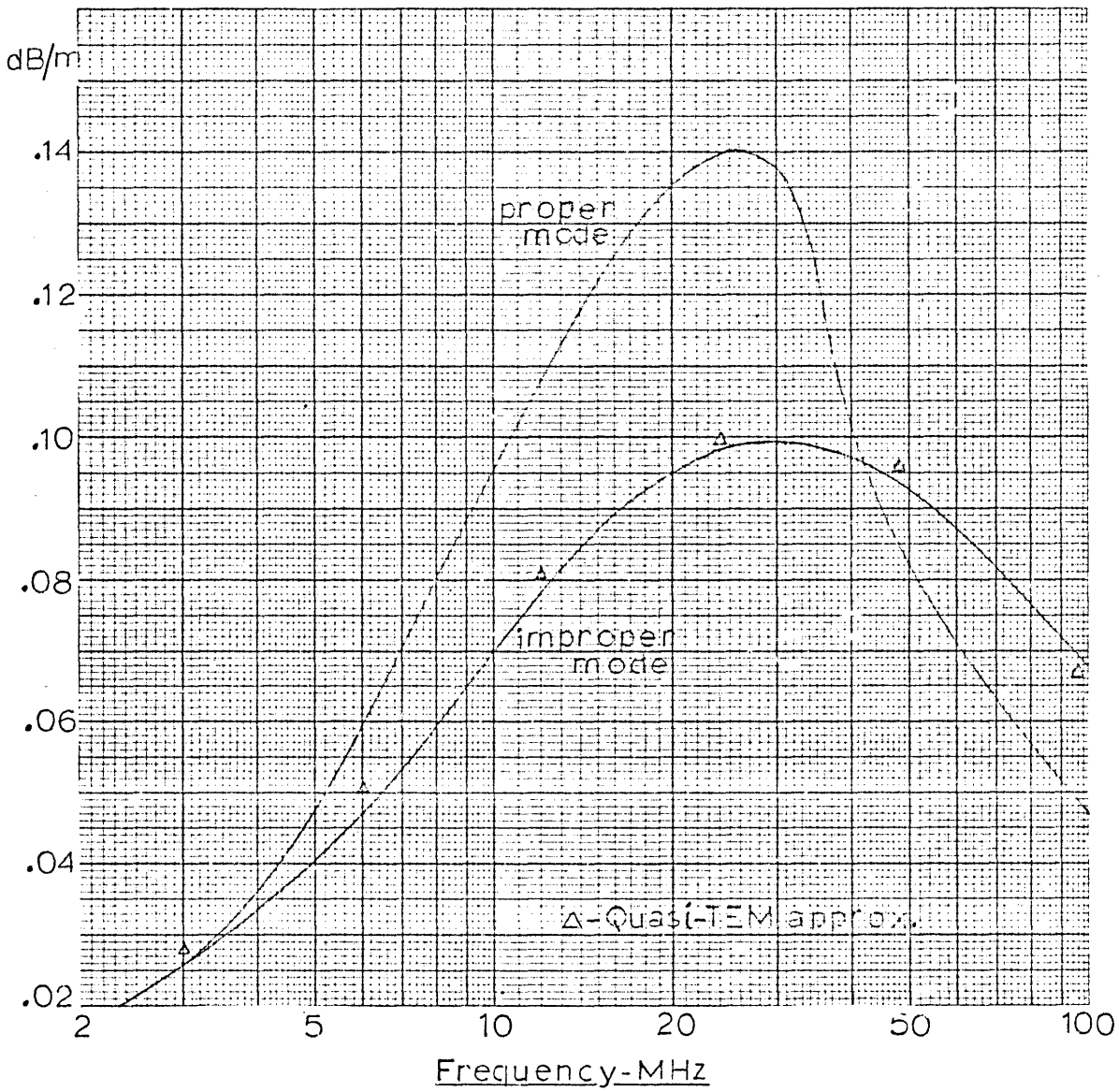
dB/m
.14
.12
.10
.08
.06
.04
.02
proper mode
improper mode
Δ-Quasi-TEM approx.
2
5
10
20
50
100
Frequency-MHz

Fig. 2.6

two modes and the quasi-T.E.M solution (See following Table) also supports this conclusion although the deviation between the quasi-T.E.M solution and the proper mode is less marked than in the case of the attenuation constant.

$$\text{Velocity ratio} = \frac{\text{phase velocity}}{\text{velocity of light in dielectric}}$$

Frequency MHz	Quasi-T.E.M	Proper mode	Improper mode
3.0	.938	.934	.938
6.0	.961	.955	.959
12.0	.983	1.003	.980
24.0	.998	1.004	.995
48.0	1.003	1.007	1.001

Incidentally, in the case of the proper mode we have done a direct integration along the real axis in the S plane as well as an integration along the steepest-descent path. This confirmed that no contribution from the poles had to be added to the steepest-descent integral and showed that, for the same accuracy, the computer time required for integration along the real axis was

three times greater*.

The question that the numerical results cannot resolve is which of the two possible solutions leads to results closer to the propagation constant measured in a real structure. It seems to us, however, that the excitation of one mode or the other should depend entirely on the launching device that is used. If the structure is energised by a voltage generator connected between the wire and the ground, it appears reasonable to expect that, above the wire, the field will be composed of outgoing plane waves in which case the corresponding solution of Maxwell's equations for the infinitely long structure is the improper mode.

---

* The time required for calculating (by the iterative method) one value of the propagation constant to an accuracy of 10^{-4} was about 0.8s on the CDC6600 computer. In the case of the quasi-T.E.M approach it was 0.01s using a 15-point Gauss formula which gives an accuracy ranging from 10^{-4} to 10^{-2}.

2.7. Measurement of the Propagation Constant

As far as we are aware no experimental results have been published regarding the electromagnetic wave propagation in the structure analysed in the preceding sections. Thus, to verify the validity of the theory we devised the experimental model described below and measured the propagation constant for two different launching devices.

2.7.1. Experimental Model

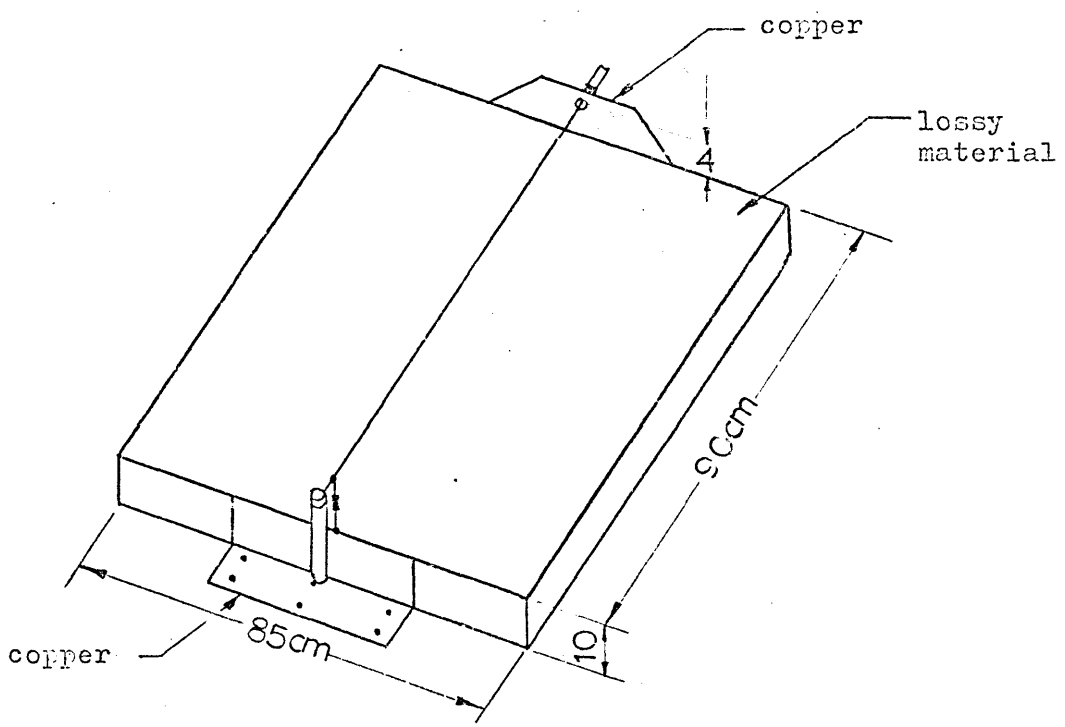

Fig. 2.7

To permit making the measurements in the laboratory the

small-size model shown in Fig.2.7 was built. The ground is represented by a slab of lossy material consisting of polyurethene foam impregnated with aquadag solution (suspension of graphite in water). The dielectric constant of this material is about 7 and its conductivity is of the order of 0.1 S/m. The propagation constant was measured at several frequencies covering the range 600 to 1800 MHz. Two different launching devices were used: one is simply a vertical wire connecting the generator between the ground and the horizontal wire (this will be referred to as LD1) and the other is a coaxial connector inserted in a vertical copper plate (LD2) as shown in Fig.2.7.

The thickness of the lossy medium is greater than its skin depth only above 700 MHz. However, a measurement of the surface impedance showed that, within the frequency range 600-1800 MHz, the finite thickness of the lossy medium does not affect the impedance measured at the interface between that medium and the air (See section 2.7.3). Hence for the above-mentioned frequency range the model of Fig.2.7 should be an accurate representation of the structure considered in the theoretical study.

2.7.2. Measuring Technique

Two methods for measuring the propagation constant were considered: (a) Measurement of the input impedance for short circuit and open circuit terminations; (b) Measurement of the wavelength

and attenuation constant by means of a movable probe exploring the field in the axial direction.

The first method was rejected as it would be subject to significant errors arising from the perturbation of the field in the vicinity of the junction between the coaxial cable and the lossy line, and from the fact that a good open-circuit termination is very difficult to realise.

The second method involves measuring separately the wavelength and the attenuation constant. The wavelength is measured as in a standard slotted coaxial line by determining the distance between two successive minima of the standing-wave pattern with the line terminated in a reactive load*. The attenuation constant is obtained from a plot of field strength (in logarithmic units) against distance along the line (See Fig. 2.8) when it is terminated in a nearly-matched load.

The probe used for these measurements is represented in Fig.2.9. It is constituted by a short vertical antenna mounted on a small copper plate, and connected to a receiver by means of a thin (2mm in diameter) flexible coaxial-cable. The probe slides on the surface of the lossy material and its position along the transmission line is controled by a nylon string and a system of pulleys.

---

* The distance between two adjacent minima is slightly different from $\lambda/2$ but since $\alpha \ll \beta$ the error is negligible.

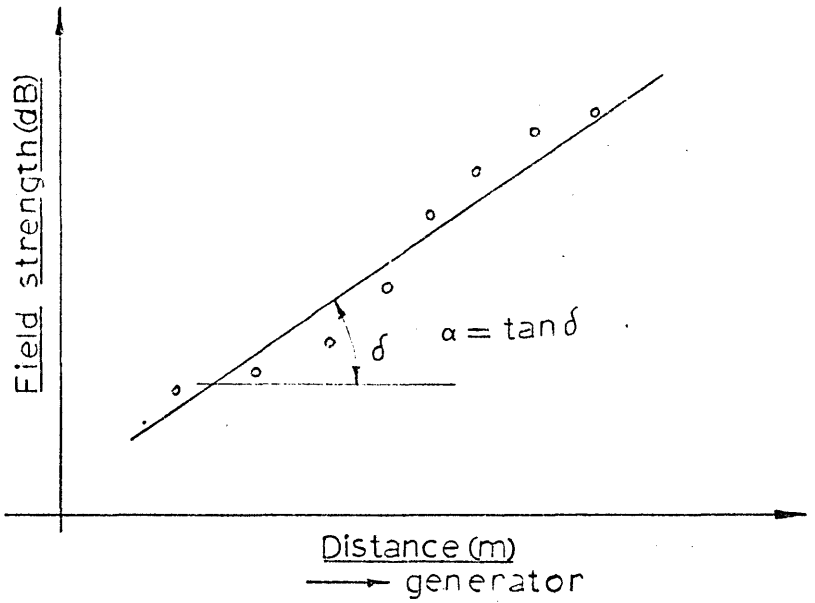
Field strength(dB)
α = tan δ
δ
Distance (m)
generator

Fig. 2.8

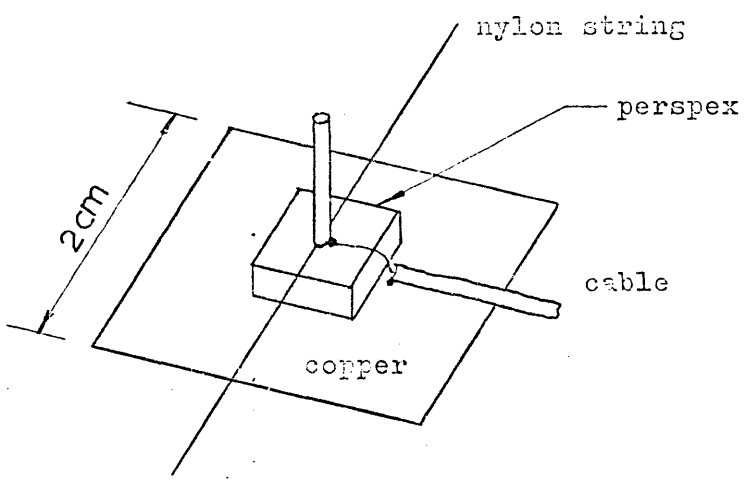
nylon string
perspex
2cm
cable
copper

Fig. 2.9

The possibility of measuring the field by using a modulated-perturbation technique[16] [17] was also considered. This would permit substituting the coaxial cable by a pair of high-resistance leads and thus reduce, in principle, the perturbation of the field caused by the probe. However, it was concluded that the perturbation of the field could be made sufficiently small, simply by positioning the cable in a region of weak electric field. Taking into consideration that the perturbation method is less sensitive and requires a more complicated instrumentation, we opted for the probe method.

2.7.3. Measurement of the Constants of the Lossy Material

The measurement of the dielectric constant and conductivity of the lossy material can be made by several methods an account of which is found in ref.18. Taking into consideration that the material exhibits high losses and that the measurements must be made over a wide frequency band (600-1800 MHz) the method of Roberts and von Hippel[19] was chosen. This method consists in measuring the impedance of a section of short-circuited transmission line (or waveguide) filled with the lossy material (Fig.2.10). The constants of the material are then calculated from the measured impedance.

Assuming a T.E.M. mode and denoting by R the reflection coefficient at the interface I as measured in the slotted line, we

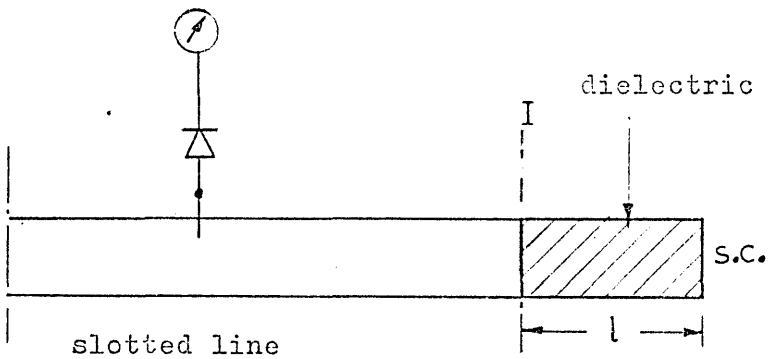

Fig. 2.10

have:

$$R = \frac{Z_I - Z_o}{Z_I + Z_o}$$

or

$$\frac{Z_I}{Z_o} = \frac{1+R}{1-R} \qquad (41)$$

where $Z_o = \sqrt{\mu_o / \epsilon_o}$ and Z_I is the impedance of the section of dielectric-filled transmission line, measured at the interface. Z_I is related to the propagation constant inside the sample (γ_d) by (19)

$$\frac{Z_I}{Z_o} = \frac{jk_o}{\gamma_d} \tanh \gamma_d l$$

Substitution in (41) gives

$$\frac{1+R}{1-R} = j\frac{k_o}{\gamma_d}\tanh\gamma_d l \qquad (42)$$

If $\text{Real}\{2\gamma_d l\} \ll 1$ this expression reduces to

$$\frac{1+R}{1-R} \simeq j\frac{k_o}{\gamma_d} = \frac{1}{n} \qquad (43)$$

n being the refractive index of the material.

The validity of this approximation can be checked by varying the position of the short circuit relative to the sample and determining whether the reflection coefficient changes. If no measurable change occurs we can conclude that the sample behaves as if its thickness were infinite.

Because of the difficulty in cutting samples in coaxial shape, the impedance measurements were made in a strip line (strip width = 80mm, distance between strips = 11mm). This is not a closed structure but providing the strip width is much greater than the distance between strips, no significant errors should result.

2.7.4. Results

The dielectric constant and conductivity of the lossy material are plotted against frequency in Fig.2.11. The high dielectric constant is probably due to the material being constituted by particles of carbon which act as small electric dipoles. A similar behaviour is reported in ref.20 in the case of carbon particles

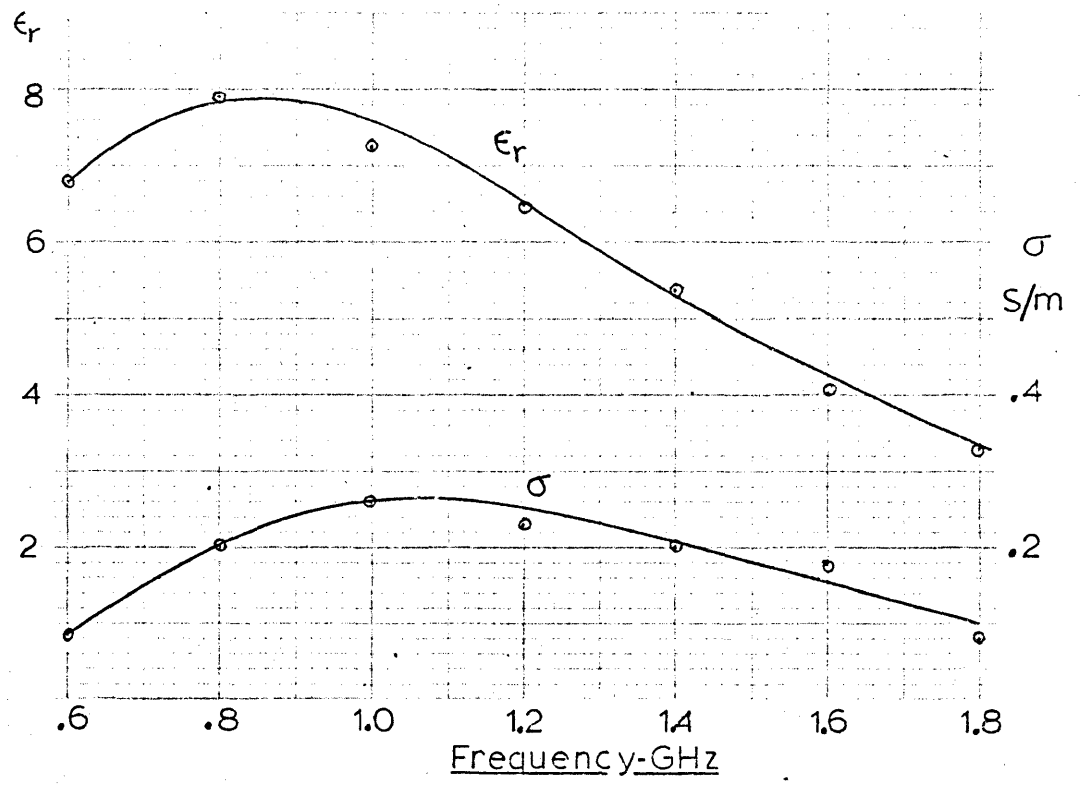

Fig. 2.11

embedded in rubber. It is to be expected that in such cases the constants of material should depend on the frequency.

In Fig.2.12 the attenuation constant for the structure of Fig. 2.7 is plotted as a function of the frequency for the two launching devices referred to in section 2.7.1. For comparison, the theoretical results for the proper and improper modes are plotted in the same diagram.

An examination of Fig.2.12 suggests the following remarks:

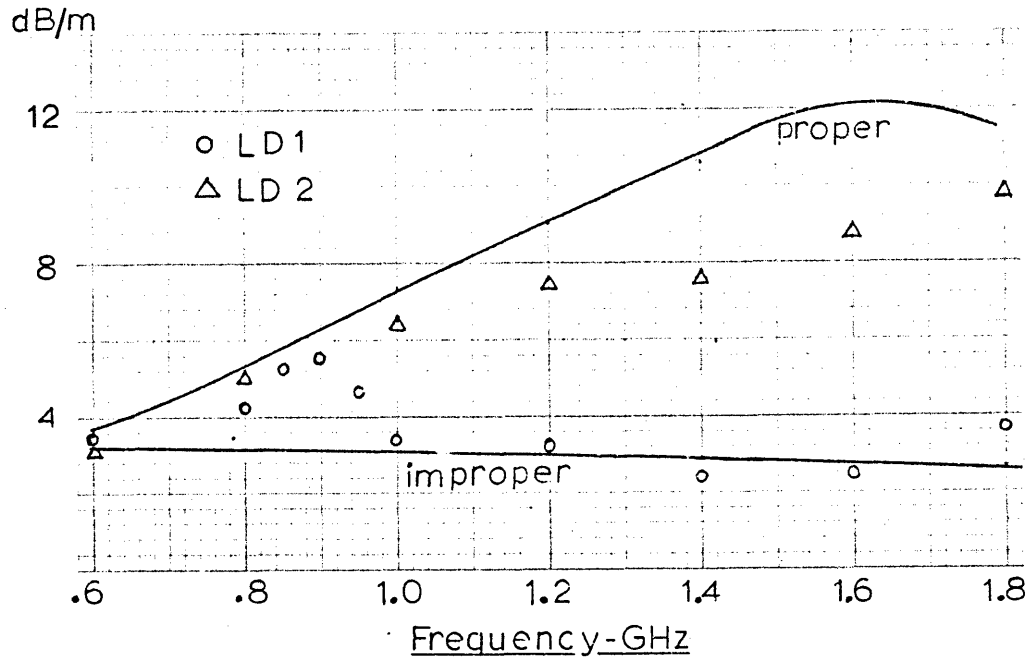

Fig. 2.12

(a) For LD1 the experimental values lie close to the curve corresponding to the improper mode except for frequencies near 900 MHz. This appears to confirm our conclusion that if the generator is located between the wire and the ground, as in the Beverage antenna, the field should correspond to the improper solution of the wave equation.

(b) For LD2 the experimental values lie nearer to the curve for the proper mode but are somewhat deviated from it. This can only be interpreted as indicating that both modes are excited, the proper

mode being predominant. In a sufficiently long structure it should be possible to distinguish the presence of two modes since at large distances from the generator the proper mode becomes negligible because of its higher attenuation constant. The structure of Fig.2.7 is relatively short and the results are probably a weighted average of the attenuation constant for the two modes.

(c) The fact that the experimental values for LD1 deviate from the curve for the improper mode at about 900 MHz may indicate a conversion of energy from one mode to the other, as they have nearly-equal propagation constants and therefore must have similar field structures.

As far as the phase velocity is concerned the measured values for both lauching devices vary from 97% to 98% of the velocity of light in free space which is about 3% less than the value given by the theory. The difference is probably due to the finite surface impedance of the copper wire.

To conclude we can say that, although the question of excitation of the proper mode would require further study, in regard to the problem of calculating the propagation constant of the Beverage antenna, the experimental results confirm that the quasi-T.E.M. formula 37 is applicable and sufficiently accurate.

2.8. Characteristic Impedance

Thus far we have been concerned with determining the propagation constant of the lossy transmission line constituted by the horizontal wire and the ground. In this section we consider the the calculation of the characteristic impedance.

In the case of an ideal transmission line the characteristic impedance is defined as the ratio of the voltage between the two conductors that form the line, to the current flowing in them. However, in the structure under consideration the voltage depends on the integration path and, as a result, the characteristic impedance is not uniquely defined. A possible definition is

$$Z_c = -\frac{1}{I}\int_0^{b-a} E_y dy \qquad (44)$$

The evaluation of this expression is in principle straightforward but involves a great deal of computational work.

It is known from practical experience that the characteristic impedance does not differ significantly from that of the lossless line obtained by considering the ground as perfectly conducting, i.e.

$$Z_c = \frac{Z_o}{2\pi} \ln\frac{2b}{a} \qquad (45)$$

In the subsequent sections of this thesis the characteristic

impedance is used only in calculating the gain of the Beverage antenna in which case the accuracy of the approximate formula 45 is adequate. Hence no further consideration is given to the evaluation of (44).

Appendix 1

Solution of Non-Homogeneous Two-Dimensional Helmoltz Equation

To solve the non-homogeneous differential equation 7 we express Φ_{10} and $\delta(x)$ in the form

$$\Phi_{10} = \int_C \mathcal{F}_{10} e^{-jsx}\, ds \qquad (A.1)$$

$$\delta(x) = \frac{1}{2\pi} \int_C e^{-jsx}\, ds$$

and substitute these expressions in eq.7. After differentiating under the integral sign we obtain

$$\int_C \left[\frac{d^2 \mathcal{F}_{10}}{dy^2} + u_1^2 \mathcal{F}_{10} - j \frac{I}{2\pi\omega\epsilon_o} \delta(y-b) \right] e^{-jsx}\, ds = 0$$

which is satisfied if

$$\frac{d^2 \mathcal{F}_{10}}{dy^2} + u_1^2 \mathcal{F}_{10} = j \frac{I}{2\pi\omega\epsilon_o} \delta(y-b) \qquad (A.2)$$

Appropriate solutions of this equations are

$$\mathcal{F}_{10} = \begin{cases} A\, e^{-ju_1 y} & y > b \\ B\, e^{ju_1 y} & y < b \end{cases} \qquad (A.3)$$

where A and B are constants. Integration of (A.2) between b-0 and b+0 yields

$$\left.\frac{d\mathcal{F}_{10}}{dy}\right|_{b_-}^{b_+} = j\frac{I}{2\pi\omega\epsilon_o}$$

in which use has been made of the continuity of $\mathcal{F}_{10}$. Thus

$$Ae^{-ju_1 b} - Be^{ju_1 b} = 0$$

$$-u_1(Ae^{-ju_1 b} + Be^{ju_1 b}) = \frac{I}{2\pi\omega\epsilon_o}$$

Solving for A and B and substituting in (A.3)

$$\mathcal{F}_{10} = -\frac{I}{4\pi\omega\epsilon_o u_1} e^{-ju_1|y-b|} \qquad (A.4)$$

Writing $x=R_1\sin\theta$, $y-b=R_1\cos\theta$ and using the transformation (14) we obtain from (A.1) and (A.4)

$$\frac{4\omega\epsilon_o}{I}\Phi_{10} = -\frac{1}{\pi}\int_C e^{-jh_1R_1\cos(\varphi-\theta)}\,d\varphi$$

$$= -\frac{1}{\pi}\int_C e^{-jh_1R_1\cos\varphi}\,d\varphi$$

By comparing this expression with the definition of the Hankel functions of zero order[9] we recognise that

$$\frac{4\omega\epsilon_o}{I}\Phi_{10} = \begin{cases} -H_o^{(2)}(h_1R_1) & \text{for } C\equiv C_i \\ H_o^{(1)}(h_1R_1) & \text{for } C\equiv C_p \end{cases} \qquad (A.5)$$

Appendix 2

Integration along the Steepest -Descent Contour

Consider the integral

$$G = \int_{C_i} g(u_1) e^{-ju_1 d}\, ds$$

$$= h_1 \int_{SDC} g(h_1 \cos\varphi)\cos\varphi\, e^{-jh_1 d\cos\varphi}\, d\varphi \qquad (32')$$

in which the exponent in the integrand has a saddle point at $\varphi = 0$. Noting that on the steepest-descent contour $\mathrm{Im}\{-h_1 d\cos\varphi\} = \text{const.} = \mathrm{Im}\{-jh_1 d\}$, we write (ref.5 section 3.1)

$$-jh_1 d\cos\varphi = -jh_1 d + 2jh_1 d \sin^2\frac{\varphi}{2}$$

$$= -jh_1 d - t^2$$

i.e. the change of variable

$$t = -j\sqrt{2jh_1 d}\, \sin\frac{\varphi}{2} \qquad (A.6)$$

$$d\varphi = \frac{2j}{\sqrt{2jh_1 d + t^2}}\, dt$$

transforms the steepest-descent path in the φ plane into the real axis in the t plane; thus

$$G = 4jh_1 e^{-jh_1 d} \int_0^\infty \frac{g(h_1 \cos\varphi)\cos\varphi}{\sqrt{2jh_1 d + t^2}} e^{-t^2} dt \qquad (38)$$

where

$$\cos\varphi = 1 - j\frac{t^2}{h_1 d}$$

Similarly for the proper mode we have

$$G = 4h_1 e^{jh_1 d} \int_0^\infty \frac{g(-h_1 \cos\varphi')}{\sqrt{2jh_1 d - t^2}} e^{-t^2} \cos\varphi' \, dt \qquad (38')$$

where

$$\cos\varphi' = 1 + j\frac{t^2}{h_1 d} .$$

References

1. J.R.Carson "Wave propagation in overhead wires with ground return" Bell System Technical Journal Vol.5 p.539, 1926.

2. F.Pollaczek "Uber das Feld einer unendlich langen wechselstromdurchflossenen Einfachleitung" Elektrische Nachriten Tecknick Vol.3 p.339, 1926.

3. W.H.Wise "Propagation of high-frequency currents in ground return circuits" Proc. I.R.E. Vol.22 p.522, 1934.

4. H.Kikuchi "Wave propagation along infinite wire above ground at high frequencies" Electrotechnical Journal of Japan, December 1956 p.73.

5. J.Zucker "Surface-wave and leaky-wave antennas" Antenna Engineering Handbook" ED.H.Jasik, section 16.2, McGraw-Hill, 1961.

6. A.Banos, Jr. "Dipole radiation in the presence of a conducting half-space" Pergamon Press 1966.

7. C.C.Johnson "Field and wave electrodynamics" McGraw-Hill 1965, section 1.15.

8. R.E.Collin "Field theory of guided waves" McGraw-Hill 1960, section 11.8.

9. G.Carrier, M.Krook, C.Pearson "Functions of a complex variable:

theory and technique" McGraw-Hill 1966, section 5.5.

10. R.H.Lien "Radiation from a horizontal dipole in a semi-infinite dissipative medium" J.Appl. Physics, Vol. 24 p.1, 1953.

11. P.Bannister "The quasi-near field of dipole antennas" I.E.E.E. Trans. on Antennas and Propagation Vol. AP-15 p.618 1967.

12. "Handbook of mathematical functions" Ed. M.Abramowitz and I. Stegun, Dover 1965, Ch.9.

13. Z.Kopal "Numerical analysis" Chapman & Hall 1961, section VII. G and appendix IV.

14. P.Henrici "Elements of numerical analysis" John Wiley 1964, Ch.4.

15. R.E.Esch "The instability of a shear layer between two parallel streams" J. Fluid Mechanics Vol.3 p.289, 1957.

16. J.H.Richmond "A modulated scattering technique for measurement of field distributions" I.R.E. Trans. on Microwave Theory and Techniques, Vol.MTT. 3 p.13 July 1955.

17. R.J.King "An amplitude and phase measuring system using a small modulated scatterer" Microwave Journal Vol.8 p.51 March 1965.

18. Handbook of Microwave Measurements, Vol. II, Ch.IX', Ed: M. Sucher and J.Fox, Polytechnic Press.

19. S.Roberts and A.von Hippel "A new method for measuring dielectric constant and loss in the range of centimeter waves" Journal of

Applied Physics Vol.17 p.610, 1946.

20. "Microwave transmission circuits" Ed. G.Ragan, Dover 1965, section 3.9.

3. THE BEVERAGE ANTENNA

3.1. Introduction

The Beverage antenna, represented schematically in Fig.3.1, consists of a horizontal wire situated at low height above ground ($b/\lambda \ll 1$) and terminated in the characteristic impedance of the lossy transmission line constituted by the wire and the ground. It was developed in 1923 by Beverage, Rice and Kellogg[1] for ground-wave reception in the long and medium wave bands. This antenna depends for its operation on the existence of a finite component of the electric field parallel to the wire and this implies that it must operate over a moderately conducting ground.

Because of the inevitable loss in the ground, the Beverage antenna has a relatively low efficiency (ranging from about 1% to about 20% depending on the antenna dimensions and ground constants) but this is no great disadvantage if it is used for receiving signals in the frequency range where the external noise level is high. On

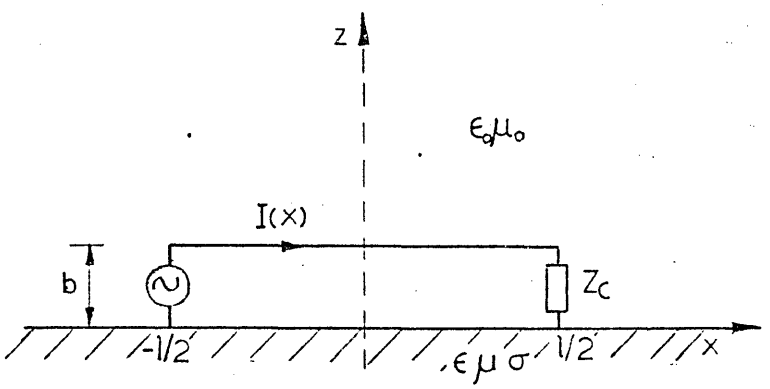

Fig. 3.1

the other hand its constructional simplicity, wide-band characteristics and good side-lobe performance make it an attractive proposition as a receiving antenna. Nevertheless, it is not as widely used as other types of receiving antenna whose radiation patterns exhibit substantially higher side lobes. And it appears that it is still mainly regarded as a low-frequency or medium-frequency antenna[2] [3].

As far as we are aware only two papers on the Beverage antenna[1][4] have been published. Both papers deal with the characteristics of the Beverage as a ground-wave antenna.

In this chapter we determine the characteristics of the Beverage as an antenna for sky-wave reception or transmission, and discuss ways of improving its performance, in particular, by using

multi-wire structures.

Although the Beverage is mainly used for reception because of its low absolute gain, we deal with the transmitting antenna as most antennas are analysed from this point of view (See for example refs.2 and 3).

3.2. Evaluation of the Far Field

Consider a Beverage antenna extending from $x=-l/2$ to $x=l/2$ along the x axis (Fig.3.1). Let $I_o \exp\{-\gamma x\}$ be the current in the horizontal wire due to a generator at $x=-l/2$. To determine the far field we apply Lorentz reciprocity theorem to the fields of the antenna and of an auxiliary electric or magnetic current element located at the observation point[5][6]. Denoting by $\bar{E}$, $\bar{H}$ the field of the antenna and by $\bar{E}_a$, $\bar{H}_a$ the field of the auxiliary current, the reciprocity relation is written[6]:

$$\oint_S (\bar{E} \times \bar{H}^a - \bar{E}^a \times \bar{H}) \cdot \bar{n} \, dS = \int_V (-\bar{E} \cdot \bar{J}^a + \bar{H} \cdot \bar{K}^a) dV \qquad (1)$$

where $\bar{J}, \bar{K}$ denote electric and magnetic current densities and $\bar{n}$ is the outward normal to the surface S bounding the volume V. It is assumed that S has been chosen so that it does not enclose the antenna structure (See Fig.3.2.) i.e. the volume V does not contain the sources of the field $\bar{E}, \bar{H}$. In this case we can take, for

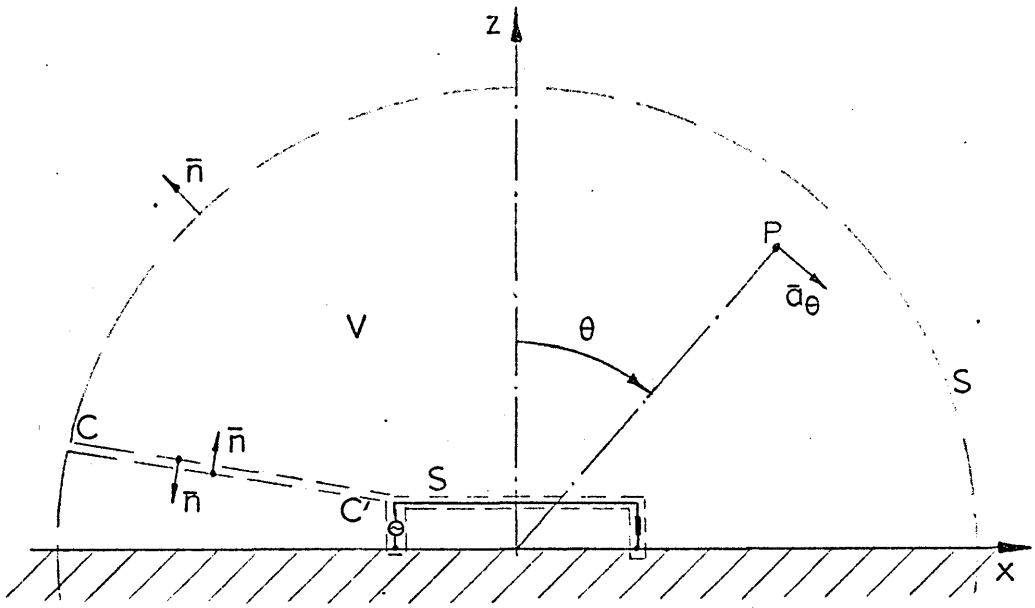

Fig. 3.2

$\bar{E}^a$ $\bar{H}^a$, the field of a current element radiating in the absence of the antenna since it satisfies Maxwell's equations within the volume V.

When $\bar{K}^a=0$ (electric current element) eq.1 yields the vertically-polarised component of the antenna field; $\bar{J}^a=0$ (magnetic current element) yields the horizontally-polarised component.

It is to be noted that the only non-vanishing contribution to the surface integral in eq.1 comes from the antenna surface since both fields satisfy the radiation condition[7] and the

contribution from the cut CC' is obviously zero. In addition, assuming that the antenna surface is perfectly conducting the first term in the surface integral vanishes. Hence eq.1 reduces to

$$-\oint_{S_a} \bar{E}^a \, \bar{H}.\bar{n}\,dS = \int_V (-\bar{E}.\bar{J}^a + \bar{H}.\bar{K}^a)\, dV \qquad (2)$$

S_a being the antenna surface. Neglecting the contribution to the surface integral from the vertical terminations (this is computed in section 3.4) and assuming an infinitely thin wire, eq.2 yields, for a current element parallel to $\bar{a}_\theta$, the following relations:

$$I_o \int_{-1/2}^{1/2} E_x^a \exp\{-\gamma x\} dx = I^a \delta l^a E_\theta \qquad (\bar{K}^a=0) \qquad (3.a)$$

$$= -M^a \delta l^a H_\theta \qquad (\bar{J}^a=0) \qquad (3.b)$$

where $I^a \delta l^a$ and $M^a \delta l^a$ are the moments of the electric and magnetic current elements respectively.

The field E_x^a is given by the following expressions (See Appendix):

Electric current element:

$$E_x^a = -j \frac{Z_o}{2\lambda} I^a \delta l \cos\phi \cos\theta \,(1-R'_V)\, q(r,b) e^{jk_o x \cos\phi \sin\theta} \qquad (4)$$

$$q(r,b) = \frac{1}{r} e^{-j(k_o r - b\cos\theta)} \qquad R'_V = R_V e^{-2jk_o b\cos\theta} \qquad (5)$$

Magnetic current element:

$$E_x^a = j \frac{1}{2\lambda} M^a \delta l \sin \phi \, (1+R'_H) q(r,b) e^{jk_o x \cos \phi \sin \theta} \qquad (6)$$

$$R'_H = R_H \, e^{-2jk_o b \cos\theta} \qquad (7)$$

where

$$Z_o = \sqrt{\frac{\mu_o}{\epsilon_o}} \qquad k_o = \frac{2\pi}{\lambda}$$

and R_V and R_H are Fresnel reflection coefficients for vertical and horizontal polarisations respectively.

By substituting (4) and (6) in (3) and integrating, we obtain

$$E_\theta = -jV_o \cdot \frac{\sin(X-ja)}{X-ja} \cos \phi \cos\theta \, (1-R'_V) \, q(r,b) \qquad (8.a)$$

$$E_\phi = jV_o \cdot \frac{\sin(X-ja)}{X-ja} \sin \phi \, (1+R'_M) \, q(r,b) \qquad (8.b)$$

in which

$$V_o = \frac{I_o Z_o}{2} \cdot \frac{l}{\lambda}$$

$$X = \frac{l}{\lambda}(\beta/k_o - \cos \phi \sin\theta) \qquad a = \alpha l/2 \qquad (9)$$

and $\gamma = \alpha + j\beta$.

A quantity of practical interest which is immediately obtained from (8) is the ratio

$$\frac{|E_\phi|}{|E_\theta|} = \frac{|\tan\phi|}{\cos\theta} \cdot \frac{|1+R'_H|}{|1-R'_V|} \qquad (10)$$

For $b/\lambda \ll 1$ and $|n| \gg 1$ (where n is the refractive index of the ground) we have

$$1+R'_H \simeq 1+R_H \simeq \frac{2\cos\theta}{n+\cos\theta}$$

$$1-R'_V \simeq 1-R_V \simeq \frac{2}{1+n\cos\theta}$$

and substituting in (10)

$$\frac{|E_\phi|}{|E_\theta|} \simeq |\tan\phi| \cdot \frac{|1+n\cos\theta|}{|n+\cos\theta|}$$

which shows that the vertically polarised component of the radiated field is predominant for low elevation angles except for directions close to the plane $\phi = \pi/2$. But if a high degree of polarisation purity is desired a relatively high refractive index ($|n|^2 \gg 1$) is required.

3.3. Radiation Patterns

The radiation patterns of the Beverage antenna are readily obtained from eqs.8. For the predominant polarisation eq.8.a gives

Horizontal Pattern ($\theta = \theta_M$, $E(0, \theta_M) = E_{Max.}$)

$$F_1(\phi) = \left[\frac{\sin^2 X + \sinh^2 a}{x^2 + a^2}\right]^{1/2} \cos\phi \qquad (10.a)$$

Vertical Pattern ($\phi=0$)

$$F_2(\theta) = \left[\frac{\sin^2 X+\sinh^2 a}{X^2+a^2}\right]^{1/2} \cdot \left|1-R'_V\right| \cos\theta \qquad (10.b)$$

If $a \ll 1$

$$\left[\frac{\sin^2 X+\sinh^2 a}{X^2+a^2}\right]^{1/2} \simeq \frac{\sin X}{X}$$

which is the radiation pattern of an end-fire arrangement of omni-directional sources. The factor $\cos\phi$ affects the horizontal pattern in two ways; in the case of short antennas it reduces the beam-width imposing an upper limit of 90 degrees; in the case of long antennas it reduces the side lobes in the region at right angles to the main beam. An example of the pattern $F_1(\phi)$ for $l/\lambda = 3$ $\beta/k_o \simeq 1$ $a \ll 1$ is given in Fig.3.3.

We shall now examine the opposite possibility: $a \gg 1$. In this case*

$$\left[\frac{\sin^2 X+\sinh^2 a}{X^2+a^2}\right]^{1/2} \simeq \frac{\sinh a}{\left[X^2+a^2\right]^{1/2}}$$

---

* It should be noted that, if we let l tend to infinity, the radiated field remains finite. Since a current distribution of the form $I_o \exp\{-\gamma x\}$ has been used to derive eqs.8, these must be multiplied by $\exp\{-\gamma l/2\}$ before the limit is taken, in order that the power supplied by the generator should be finite.

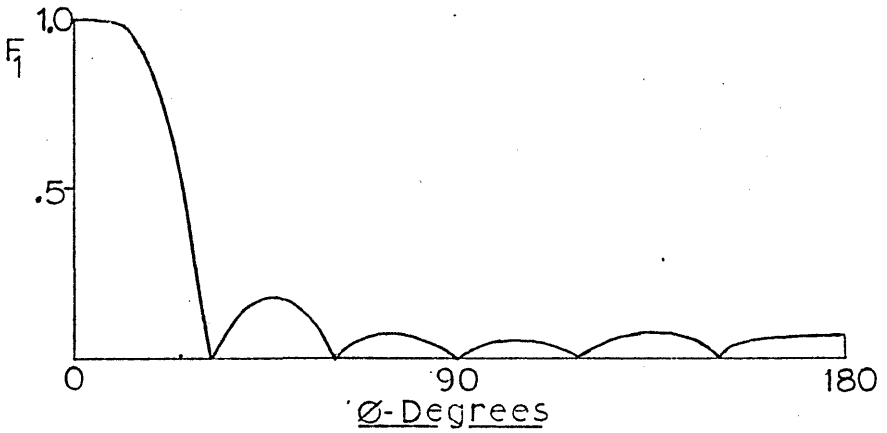

Fig. 3.3

– and the radiation pattern $F_1(\emptyset)$ has the shape of Fig.3.4. with only two lobes. If $\beta \simeq k_o$ the 3-dB points occur for $X \simeq a$ i.e.

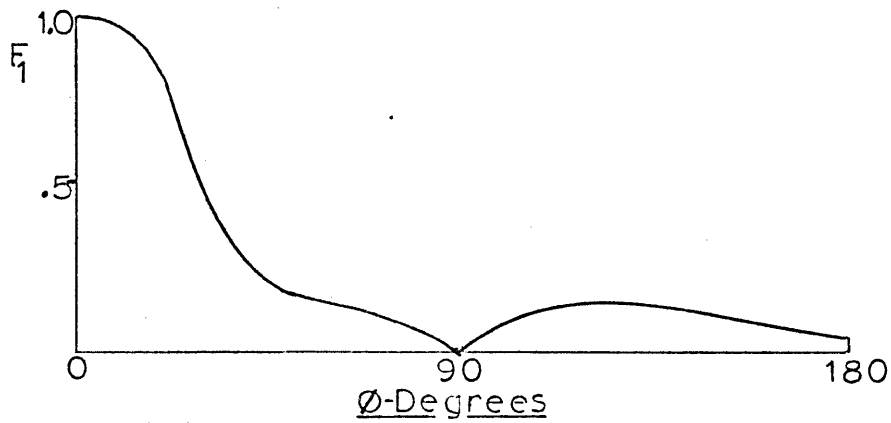

Fig. 3.4

$$\cos\phi \simeq \frac{\beta - \alpha}{k_o}$$

If α is proportional to frequency the antenna has constant beam-width but this is of little practical importance because such an antenna would be very inefficient.

3.4. Field Radiated by the Terminal Wires

Thus far, we have assumed that the field radiated by the vertical wires at both ends of the antenna is negligible compared with that due to the horizontal wire. However, this is not true in general, and to prevent a serious degradation of the radiation patterns proper attention must be paid to this problem in the design of the antenna.

In order to simplify the computations we shall assume that the height is much less than a wavelengh in which case the current in the terminal wires is approximately uniform and can be taken to be $I_o \exp\{\pm\gamma\, 1/2\}$. In fact, near the terminations the current in the horizontal wire also deviates from a pure travelling wave but if $1/b \gg 1$ this assumption should be sufficiently accurate.

The field radiated by a vertical current element of moment I.b located at the point $(x_o, 0, 0)$ is given by (3)

$$E_\theta = j \frac{IZ_o}{2r} \cdot \frac{b}{\lambda} (1+R_v) \sin\theta \, e^{jk_o x_o \cos\phi \sin\theta}$$

Taking into account that the currents in the terminal wires have opposite directions (s.Fig.3.1), the superposition of the fields gives

$$E_\theta^T = - \frac{I_o Z_o}{r} \frac{b}{\lambda} \sin (X-ja)(1+R_v) \sin\theta \qquad (11)$$

where X and a are given by expressions 9. The field E_θ^T has a number of equal maxima for the azimuthal directions that satisfy sinX=1. It can, therefore, contribute to increase the side-lobe level.

The field radiated by the horizontal wire (E_θ^H) has a maximum for $X=0$, $\phi=0$. From (11) and (8.a) we obtain

$$\rho_T \simeq \frac{|E^T|_{\sin X=1}}{|E^H|_{\sin X=0}} = \frac{2ba\sqrt{1+\sinh^2 a}}{1 \sinh a} \cdot \left| \frac{1+R_V}{1-R_V} \right| \tan\theta$$

where we have made the approximation $R_V' \simeq R_V$. If $|n| \gg 1$

$$\left| \frac{1+R_V}{1-R_V} \right| \simeq |n| \cos\theta$$

and the above expression reduces to

$$\rho_T \simeq \frac{2ba\sqrt{1+\sinh^2 a}}{1 \sinh a} |n| \sin\theta \qquad (12)$$

For $n=5$, $1/b = 100$, $a \ll 1$, $\sin\theta \simeq .9$ this expression yields

$\rho_T \simeq 0.09$ i.e. -21dB

which is considerably lower than the typical side-lobe level of the pattern $F_1(\phi)$ of Eq. 10.a.

3.5. Directivity. Gain.

3.5.1. General Considerations.

The overall performance of an antenna is usually given by two important quantities: directivity and gain. The directivity is the ratio of maximum to average radiation intensity [3],[8],

$$D = \frac{U_M}{U_{av}} \qquad (13)$$

where $U_M = \dfrac{r^2 |E_M|^2}{2Z_o}$

$$U_{av} = \frac{r^2 |E_{av}|^2}{2} = \frac{P_r}{4}$$

In the above expressions E_M is the electric field in the direction of maximum radiation and P_r is the total power radiated by the antenna.

The gain is defined as the ratio of maximum radiation intensity to the radiation intensity of a reference antenna for the same input power [3]. If the reference antenna is a lossless

isotropic source, the gain is referred to as the absolute gain [8]. Denoting by P_g the input power, the absolute gain is given by

$$G = \frac{U_M}{U_i} \qquad (14)$$

where

$$U_i = \frac{P_g}{4\pi} \qquad (15)$$

Whilst the directivity depends only on the shape of the radiation pattern, the gain is affected by the power loss in the antenna structure. In the case of a transmitting antenna the gain is a quantity of evident practical importance. In the case of a receiving antenna operating in a frequency band where the external noise level is high, the gain becomes less important and it is normally the directivity that determines the performance of the receiving system.

Denoting by S_o and N_e the signal power and external-noise power at the output of an ideal isotropic antenna, the signal-to-noise ratio at the output of an antenna of gain G and directivity D is given by*

$$\frac{S}{N} = \frac{GS_o}{\eta N_e + N_i} = D \frac{S_o}{N_e} \cdot \frac{1}{1 + N_i/\eta N_e}$$

* It is assumed that the external noise sources are uniformly distributed in the sky.

where $\eta = G/D$ is the antenna efficiency [3] and N_i is the internal noise power. The above expression shows that the improvement in signal-to-noise ratio is equal to the directivity of the antenna provided that

$$\eta N_e \gg N_i$$

The external noise power N_e depends on the time of day and season of the year. In the U.K. the lowest value of N_e is about 30dB above thermal noise level at 3MHz and 15dB at 30MHZ (See ref.9). These figures give an order of magnitude of the permissible loss $(1/\eta)$ in the antenna system* .

3.5.2. Directivity

Denoting by F_M the maximum value of the function $F_2(\theta)$ in eq. 10.b , the maximum radiated field is given by

$$|E_M| = \frac{I_o Z_o l}{2\lambda r} F_M \qquad (16)$$

from which it follows that

$$U_M = \frac{Z_o I_o^2}{8} \left(\frac{l}{\lambda}\right)^2 F_M^2 \qquad (17)$$

To obtain the average radiation intensity we calculate firstly

* In attempting a more accurate estimate of the amount of permissible loss, the receiver noise figure must be taken into account.

the power radiated by the antenna.

For vertical polarisation we have

$$P_r^{(V)} = \frac{1}{Z_o}\int_0^{\pi/2} d\theta \sin\theta \int_0^{\pi} r^2 |E_\theta|^2 \, d\phi$$

Substitution of (8.a) in this expression gives

$$P_r^{(V)} = \frac{Z_o I_o^2}{4} \left(\frac{1}{\lambda}\right)^2 I_V \qquad (18)$$

where

$$I_V = \int_0^{\pi/2} d\theta \sin\theta \cos^2\theta \, |1-R_V'|^2 \int_0^{\pi} \frac{\sin^2 X + \sinh^2 a}{X^2 + a^2} \cos^2\phi \, d\phi \qquad (19)$$

This integral is not calculable by formal analysis but can be easily evaluated numerically.

In a similar manner the power radiated with horizontal polarisation is found to be

$$P_r^{(H)} = \frac{Z_o I_o^2}{4} \left(\frac{1}{\lambda}\right)^2 I_H \qquad (20)$$

where

$$I_H = \int_0^{\pi/2} d\theta \sin\theta \, |1+R_H|^2 \int_0^{\pi} \frac{\sin^2 X + \sinh^2 a}{X^2 + a^2} \sin^2\phi \, d\phi \qquad (21)$$

By definition the average radiation intensity is given by the

equation

$$U_{av} = \frac{P_r^{(V)} + P_r^{(H)}}{4\pi}$$

which, by substituting (18) and (20) for $P_r^{(V)}$ and $P_r^{(H)}$, leads to

$$U_{av} = \frac{Z_o I_o^2}{16\pi}\left(\frac{1}{\lambda}\right)^2 (I_V + I_H) \qquad (22)$$

From (13), (17) and (22) we obtain

$$D = 2\pi \frac{F_M^2}{I_V + I_H} \qquad (23)$$

3.5.3. Absolute Gain

Taking into consideration that a current distribution of the form $I.\exp\{-\gamma x\}$ has been assumed (See section 3.2) the input power is given by

$$P_g = \frac{1}{2} Z_c I_o^2 e^{2a} \qquad (24)$$

where Z_c is the characteristic impedance of the Beverage antenna. From (15) and (24) we obtain the radiation intensity of an ideal isotropic source

$$U_i = \frac{P_g}{4\pi} = \frac{Z_c I_o^2 e^{2a}}{8\pi} \qquad (25)$$

The absolute gain G is readily obtained from (17) and (25)

$$G = \frac{U_M}{U_i} = \pi F_M^2 \left(\frac{1}{\lambda}\right)^2 \cdot \frac{Z_o}{Z_c} e^{-2a} \qquad (26)$$

G depends on the ground constants through the quantities F_M and a. An indication as to how these constants affect the gain can be obtained by considering the case $h/\lambda \ll 1$, $\alpha 1 \gg 1$, $\alpha \gg \beta - k_o \sin \theta_M$ which corresponds to a long antenna with high attenuation constant. In this case we can make the following approximations

$$e^{-a} F_M \simeq \frac{1}{2a} |1-R_V| \cos \theta_M \simeq \frac{\cos \theta_M}{a|n+\cos\theta_M|}$$

from which it follows that

$$G \simeq \frac{4\pi}{(\alpha\lambda)^2} \cdot \frac{\cos^2 \theta_M}{|n+\cos \theta_M|^2} \qquad (27)$$

Examination of this expression shows that low values of $|n|$ lead to higher gain but, since α increases with $1/n$, G varies slowly with $|n|$.

3.6. Numerical Results

In order to illustrate the performance of a Beverage antenna of typical dimensions, operating in the H.F. band we have calculated on the digital computer the main radiation characteristics of an antenna of the following dimensions:

length 300m

height 3m

wire radius 2.5mm

ground conductivity 0.01S/m

relative ground permittivity ... 15

The main results are condensed in tables I and II. The radiation patterns for vertical polarisation are represented in Fig.3.5 (pg.80).

Table I

Frequency MHz	Total Atten. dB	Gain dB	Directivity dB	Loss dB
3	4.6	-3	14	17
6	6.6	3	16	13
12	8.5	8	18	10
18	8.1	11	19	8
24	7.2	13	20	7
30	6.3	15	21	6

An examination of these results shows that:

(1) The Beverage antenna is capable of covering a very wide frequency band. The bandwidth is only limited on the low-frequency side, due to the increase in the field from the terminations relative

Table II

Frequency MHz	Horizontal Pattern		Vertical Pattern Half-power points	
	Beamwidth DEG	Side-lobe ratio dB	Lower DEG	Upper DEG
3	44	12	7	34
6	30	14	6	24
12	23	16	5	17
18	20	17	4.5	15
24	16	18	4	13
30	15	18	4	11

to the field from the horizontal wire. There appears to be no corresponding limit on the high-frequency side.

(2) The side-lobe level is substantially lower than that of a rhombic which is about -6dB (See ref. 3 chapter 14).

(3) The gain is relatively low especially at low frequencies. However this is not a serious disadvantage if the antenna is used for reception in the H.F. band. In fact, a comparison of the antenna loss (Table I) with the figures for external noise level given in section 3.5.1. suggests that no appreciable degradation of the signal-to-noise ratio is likely to result from the low efficiency of the Beverage antenna.

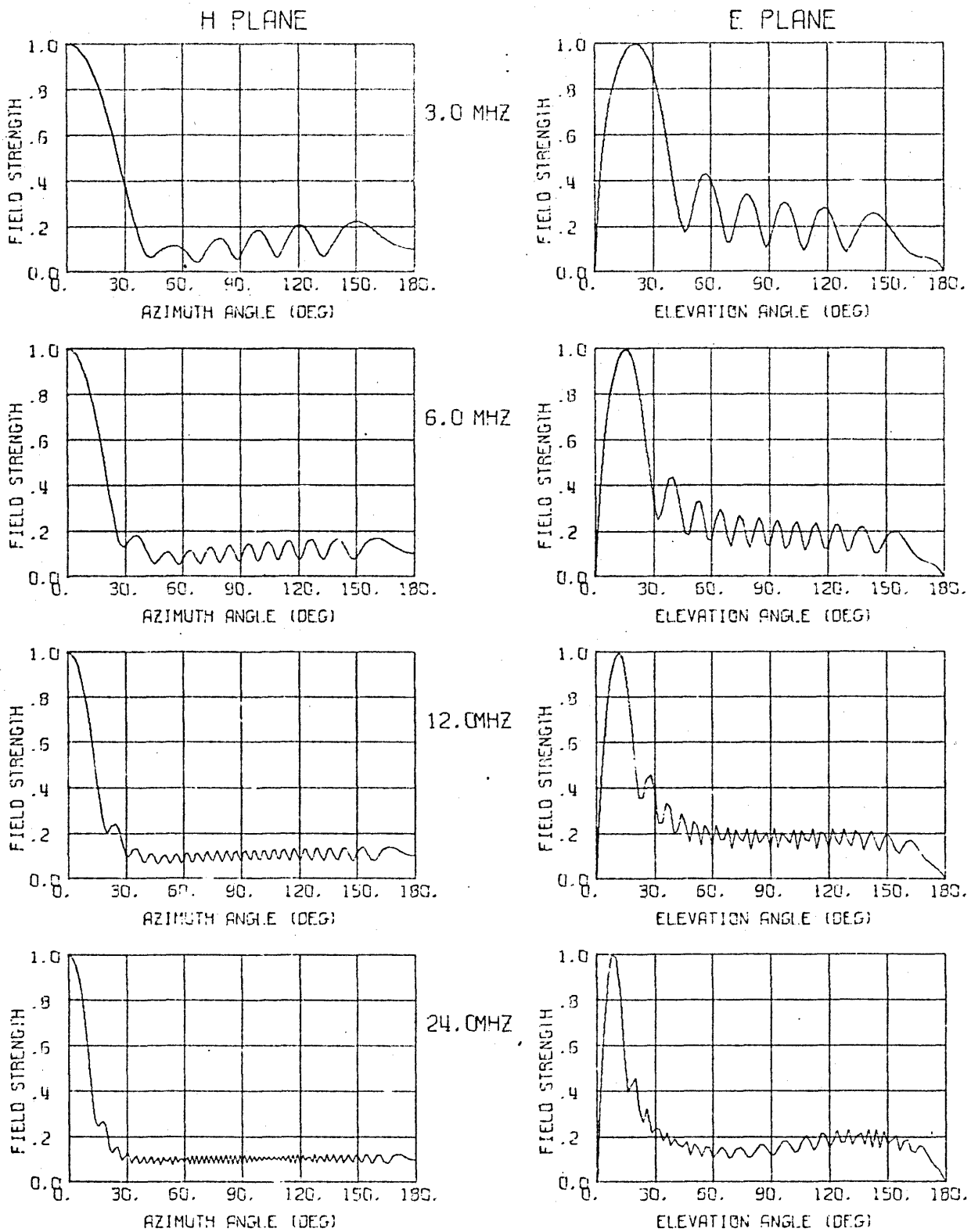

Fig. 3.5 Radiation Patterns of the Beverage antenna

3.7. Multi-Wire Structures

3.7.1. Gain and Characteristic Impedance

In this section we examine a proposal for improving the gain of the Beverage antenna. Consider the expression for the gain:

$$G = \pi F_M^2 \left(\frac{1}{\lambda}\right)^2 \frac{Z_o}{Z_c} e^{-2a} \qquad (26)$$

It is clear that G increases with $1/Z_c$ if the other quantities in (26) remain constant. However if we seek to reduce the characteristic impedance by reducing the ratio of height to wire radius, the attenuation constant will increase and no significant improvement in the gain (if any) will result. A more successful approach is to use an array of closely spaced wires as shown schematically in Fig. 3.6. By appropriately choosing the wire spacing it is possible

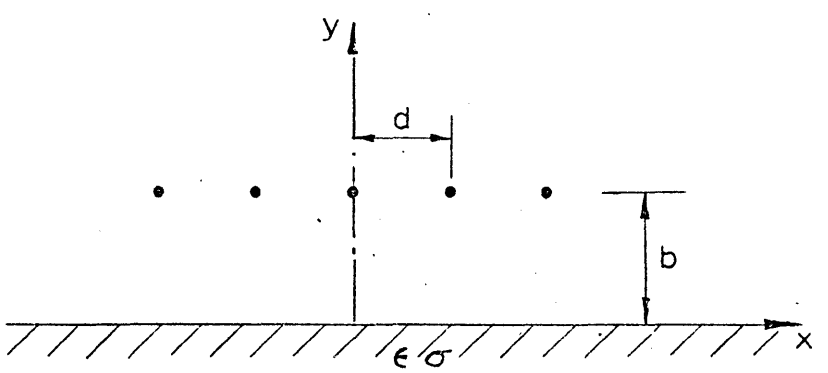

Fig. 3.6

to achieve a substantial reduction in the characteristic impedance without any appreciable increase in attenuation per unit length. The structure of Fig.3.6. is, in fact, a broadside array of Beverage aerials but if its total width is small compared with a wavelength, the directivity will not increase significantly and, therefore, the improvement in gain corresponds to an approximately equal improvement in efficiency.

It is interesting to note that Beverage, Rice and Kellogg in their original paper on the Beverage antenna[1] did consider two-wire and four-wire structures but the separation between wires was not sufficient to avoid a significant increase in the attenuation per unit length.

The calculation of the propagation constant for a system of parallel wires situated above ground is considered in the next section.

3.7.2. Propagation Constant

Consider a system of N thin wires as represented in Fig.3.6 (b/a, $d/a \gg 1$). If transverse currents on the wires are neglected, the boundary conditions on the wire surfaces reduce to (See section 2.2.)

$$E_z = 0 \quad \text{for} \quad x = \nu d \,, \; y = b - a \tag{28}$$

where ν is an integer varying from $-(N-1)/2$ to $(N-1)/2$ for an odd

number of wires. The field E_z can be written as follows:

$$E_z(x,y) = \sum_{\nu} i_\nu f_\nu(x,y) \qquad (29)$$

where f(x,y) is the z component of the electric field of a unit current situated at $x=\nu d$, $y=b$ and in presence of the ground. The functions f (x,b) can be obtained from the theory of Chapter 2.

From (28) and (29) we obtain the following set of linear equations

$$\sum_{\nu=-M}^{M} i_\nu f_\nu(\mu d, b-a)=0 \qquad (\mu=-M,-M+1,\ldots,+M) \qquad (30)$$

where $M=(N-1)/2$. The above equations can be written in matrix form

$$[F]\{I\} = 0 \qquad (31)$$

where $\{I\}$ is a column vector representing the currents and $[F]$ is a square matrix of order N whose elements are defined by

$$F_{\mu\nu} = f_\nu(\mu d, b-a)$$

The system of equations (31) has a non-trivial solution if

$$|F| = 0 \qquad (32)$$

To calculate the functions $f_\nu(x,y)$ it is sufficiently accurate to to use the quasi-T.E.M. approach. In this case the coefficients $F_{\mu\nu}$ become linear functions of $1/h_1^2$ (See sections 2.4 and 2.5.2) and thus (32) reduces to an algebraic equation of degree N in $1/h_1^2$. This means that (32) admits N solutions corresponding to N independent modes. However we are only interested in the mode for which

the phase and amplitude of the currents are approximately equal. In this case an approximation to the transverse wave number can be easily obtained by assuming equal currents and imposing the condition that the axial component of the electric field be zero on the surface of the centre wire. Eqs. 30 reduce to the single equation

$$\sum_{\nu=-M}^{M} f_\nu(0,b-a) = 0 \qquad (33)$$

The function $f_\nu(0,b-a)$ is obtained from eqs. 2.1 and 2.22*. Apart from a constant factor we have

$$f_\nu(0,b-a) = j \ln A_\nu + 2G_{1\nu} + 2jG_{2\nu}\left(1-\frac{k_o^2}{h_1^2}\right) \qquad (34)$$

$$h_1^2 = k_o^2+\gamma^2 \qquad (35.a)$$

where

$$\begin{aligned} A_\nu &= \sqrt{4b^2+(\nu\, d)^2}\,/\nu\, d \qquad \nu \neq 0 \\ &= 2b/a \qquad \nu = 0 \end{aligned} \qquad (35.b)$$

$$G_{1\nu} = \int_0^\infty \frac{e^{-2bs}}{-js+u_2} \cos \nu\, d\, ds \qquad (35.c)$$

$$G_{2\nu} = \frac{1}{k_o^2} \int_0^\infty s\, \frac{u_2+js}{-jn^2 s+u_2} \cos \nu\, d\, ds \qquad (35.d)$$

---

* When referring to equations from other chapters the first figure in the reference indicates the chapter.

Solving (33) for h_1^2 gives

$$h_1^2 = k_o^2 \frac{\sum_\nu G_{2\nu}}{\sum_\nu \left[\frac{1}{2} \ln A_\nu - jG_{1\nu} + G_{2\nu}\right]} \qquad (36)$$

This expression can be easily evaluated on the digital computer once a suitable quadrature formula for evaluating $G_{1\nu}$ and $G_{2\nu}$ has been chosen. If $\nu d/b \gg 1$ the 15-point Gauss-Laguerre quadrature formula[10] may not be accurate enough in which case it is preferable to use Simpson's rule choosing the number of points so that the desired accuracy is attained.

In order to investigate the effect of the wire spacing on the attenuation constant we calculated h_1^2 for a system of two wires and for various values of the spacing. The results are plotted in Fig. 3.7. The attenuation per unit length is greater than that for a single wire for separations up to about half wavelengh and less for greater distances. This indicates that the axial electric fields of the two currents are near anti-phase for separations greater than about half wavelength.

In Fig. 3.8 we have plotted the attenuation constant for a system of parallel wires with a spacing of two heights for an increasing number of wires. The attenuation reaches a maximum for a total width of the structure somewhat less than one wavelength which is in accordance with the results obtained for the two-wire

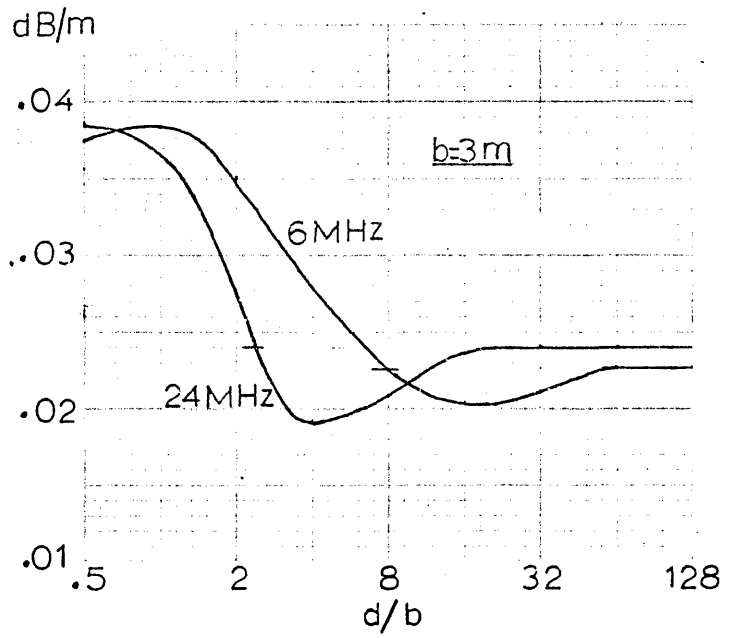
dB/m
.04
.03
.02
.01
b=3m
6MHz
24MHz
.5
2
8
32
128
d/b

Fig. 3.7

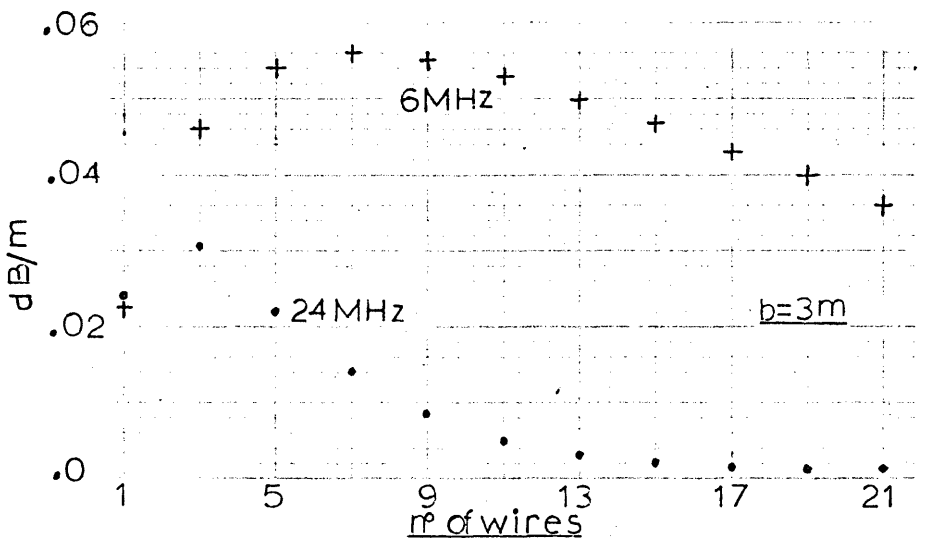
.06
.04
.02
.0
dB/m
6MHz
24MHz
b=3m
1
5
9
13
17
21
n° of wires

Fig. 3.8

system.

However, a rather unexpected result is the considerable reduction in attenuation comparing with a single wire which is shown by the 24MHz curve. Probably this indicates that as the number of wires increases the field near the ground decreases so that most of the energy flows in the vicinity of the wires.

3.7.3. Improvement in Efficiency

We are now in a position to show that by using a multi-wire structure of appropriate dimensions the efficiency of the Beverage antenna can be significantly improved. Consider a system of 11 wires with an equal spacing of 6m. The total width of this structure is 60m i.e. 1.2λ at 6 MHz. For wires six-wavelength long the directivity of the multi-wire structure, at 6 MHz, is only slightly greater than that of a single wire. Hence the increase in gain corresponds to an increase in efficiency of approximately the same magnitude. The reduction in characteristic impedance is about 9 dB but, taking into account that the factor $\exp\{-2a\}$ in eq.26 (wave attenuation at the antenna mid-point) increases by about 4 dB, the total improvement in efficiency is approximately 5 dB. This means that the efficiency of the antenna is raised from 5% (See Table I) to 15%. At 24MHz the increase in efficiency is more difficult to estimate since the increase in directivity is

not negligible. However it is useful to point out that the increase in gain would then be of the order of 12 dB, i.e. such an antenna would exhibit an absolute gain of about 25 dB.

3.8. Design Considerations

As in many other engineering problems there is no obvious choice of parameters of the Beverage antenna that optimises all its characteristics and, therefore, the design has to be done by trial and error. However some guidelines can be defined on the basis of the theory expounded in the preceding sections.

Firstly an approximate value of the antenna length can be calculated from the specified directivity or beamwidth by using approximate formulae for end-fire sources (See ref.8 section 8.3). If the antenna is to cover a wide frequency band it is useful to bear in mind that the beamwidth is approximately proportional to $1/\sqrt{f}$.

The height affects two important characteristics of the Beverage: the field due to the terminal wires and the attenuation constant. To ensure that the field from the vertical terminations is small compared with that from the horizontal wire a ratio of length to height of about a hundred is normally required. Expression 12 can be used to obtain an estimate of the relative importance of the field due to the terminations for any ratio of length to height.

Taking into consideration that the attenuation constant

increases with decreasing height the choice of the height may imply a compromise between low side lobes and high gain. One way of resolving the difficulty may be to increase the antenna length. The diameter of the horizontal wire also affects the attenuation constant; as long as the losses in the copper are negligible compared to the losses in the ground, a reduction in the wire diameter leads to a reduction in the attenuation per unit length.

Finally the possibility of using an array of parallel wires should be considered as it yields a significant improvement in gain.

3.9. Proposal for a New Antenna Related to the Beverage

In section 3.2 we have shown that the far field of the Beverage antenna is given by the general expression(3)

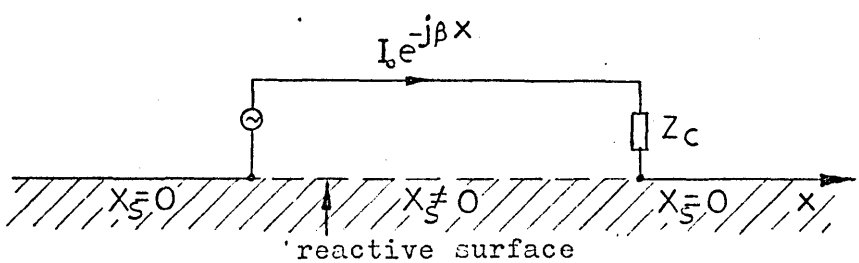

Fig. 3.9

$$E \sim \int_{-1/2}^{1/2} E_x^a \exp\{-\gamma x\}\, dx$$

where E_x^a is the electric field tangential to the wire due to a unit current element located at the observation point. The magnitude of the field radiated by the antenna depends on the magnitude of this auxiliary field. If we regard the antenna as receiving we can say that the output voltage is proportional to the voltage per unit length (E_x^a) induced on the wire by the incoming wave. To obtain a reasonable E_x^a the ground plane must exhibit a finite surface impedance of moderate value (say $Z_s > 0.1\ Z_o$). In the case of the Beverage antenna this is provided by the earth. However, it is apparent that the loss in the ground plane does not play a fundamental role in the radiation process i.e. a ground plane having a purely reactive surface impedance can be used (See Fig.3.9). This will reduce the antenna bandwidth but will eliminate the attenuation thus leading to an increase in gain. In addition, the height can be reduced as long as the velocity of propagation is not too low.

We expect that the use of a reactive ground plane in conjunction with a multi-wire upper conductor may make this antenna a practical proposition for frequencies above 100 MHz. In the high-frequency band the artificial ground plane (corrugated surface or

inductive grid) would probably be too costly.

It should be noted that if the antenna is mounted in a perfectly-conducting ground plane as indicated in Fig.3.9 an additional increase in gain relative to the Beverage will be achieved. This is due to the fact that the radiation pattern of a horizontal current element has then a maximum in the direction of its axis thus coinciding with the direction of maximum radiation of the end-fire source.

The performance of the above-proposed antenna can be determined following the method used for the Beverage antenna. To obtain the propagation constant the theory of Chapter 2 can be appropriately modified to apply to a reactive (and possibly anisotropic) ground plane. The far field can then be obtained by applying Lorentz reciprocity theorem; in the case of the structure represented in Fig.3.9 this leads to an integral over the reactive surface which may be somewhat difficult to evaluate.

Appendix

Consider an electric current element parallel to the unit vector $\bar{a}_\theta$ (Fig.A.1). At a distance R_1, large compared with a

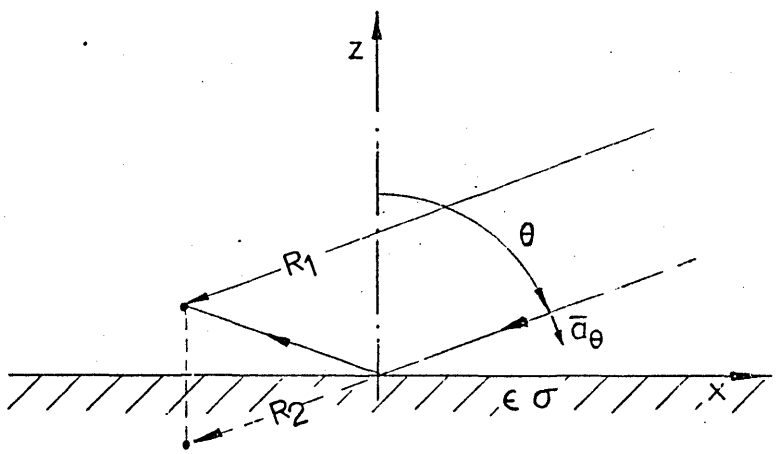

Fig. A.1

wavelength, the incident field produced by the current element is[3]

$$E_\theta^a = -j \frac{Z_o}{2\lambda} I^a \delta l \frac{e^{-jk_o R_1}}{R_1} \qquad (A.1)$$

where $I^a \delta l$ is the moment of the current element and

$$Z_o = \sqrt{\mu_o/\epsilon_o} \qquad k_o = 2\pi/\lambda$$

The total field at the observation point is expressed in terms of the incident field and the Fresnel reflection coefficient as for plane waves[11]. Hence the x component is given by

$$E_x^a = -j \frac{Z_o}{2\lambda} I^a \delta l \left[\frac{e^{-jk_o R_1}}{R_1} - R_v \frac{e^{-jk_o R_2}}{R_2} \right] \cos\phi \cos\theta \qquad (A.2)$$

in which R_v is the Fresnel reflection coefficient for horizontal polarisation[11];

$$R_v = \frac{n\cos\theta - \sqrt{1-n^{-2}\sin^2\theta}}{n\cos\theta + \sqrt{1-n^{-2}\sin^2\theta}} \qquad (A.3)$$

n being the complex refractive index of the ground given by

$$n^2 = \frac{\epsilon}{\epsilon_o} - j \frac{\sigma}{\omega \epsilon_o} \qquad (A.4)$$

For $R_1, R_2 \gg \lambda$ $x \ll R_1, R_2$

expression A.2 can be simplified by making use of the following approximations

$$\frac{1}{R_1} \simeq \frac{1}{R_2} \simeq \frac{1}{r}$$

$$k_o R_1 \simeq k_o (r - x\cos\phi \sin\theta - b\cos\theta)$$

$$k_o R_2 \simeq k_o (r - x\cos\phi \sin\theta + b\cos\theta)$$

We obtain

$$E_x^a = -j \frac{Z_o}{2\lambda} I^a \delta l (1 - R_v') \cos\theta \cos\phi \, q(r,b) e^{jk_o x c \cos\phi \sin\theta} \qquad (4)$$

where R_v' and $q(r,b)$ are given by eqs.5.

In a similar manner the field E_x^a produced by a magnetic current element parallel to $\bar{a}_\theta$ is found to be

$$E_x^a = j \frac{1}{2\lambda} M^a \delta l \, (1+R_H') \sin\phi \, q(r,b) e^{jk_o x \cos\phi \sin\theta} \qquad (6)$$

where $M^a \delta l$ is the moment of current element and R_H' is related through eq.7 to the Fresnel reflection coefficient for horizontal polarization[11],

$$R_H = \frac{\cos\theta - n\sqrt{1-n^{-2}\sin^2\theta}}{\cos\theta + n\sqrt{1-n^{-2}\sin^2\theta}} \; . \qquad (A.5)$$

References

1. H.H.Beverage, C.W.Rice and F.W.Kellogg "The wave antenna" A.I.E.E. Trans., vol.42, p.215, 1923.

2. J.D.Kraus "Antennas" McGraw-Hill, 1950 sections 14.11, 2.14 and 2.15.

3. S.A.Schelkunoff "Antennas, theory and practice" John Wiley 1952, chapters 4 and 7.

4. J.R.Wait "Radiation from a ground antenna" Canadian Journal of Technology, vol.32 p.1, January 1954.

5. A.Z.Fradin "Microwave antennas" Pergamon Press 1961, section 2.3.

6. K.Balmain "Using the reciprocity theorem for antenna calculations" Electronics Letters, vol.4 p.301, 26th July 1968.

7. R.E.Collin "Foundations for microwave engineering" McGraw-Hill 1966, section 2.12.

8. C.H.Walter "Travelling-wave antennas" McGraw-Hill 1965, section 1.2.

9. "World distribution and characteristics of atmospheric radio noise" C.C.I.R. report n^{o} 322, Geneva 1963.

10. Z.Kopal "Numerical analysis" Chapman & Hall, 1961 Appendix IV.

11. D.S.Jones "Theory of electromagnetism" Pergamon Press 1964, section 6.26.

4. The Radial Travelling-Wave Antenna

4.1. Introduction

In the two preceding chapters we have dealt with the theory of the Beverage antenna and have shown its suitability as a receiving antenna for the high-frequency band (3-30 MHz). We are now in a position to analyse the radial travelling-wave antenna which is a phase-compensated circular array of radially-arranged Beverage elements.

In section 4.2 the location of the phase centre of a travelling-wave antenna is discussed with a view to determining the phase correction to be applied to the elements of the radial travelling-wave array. In sections 4.3 to 4.5 we examine how the different parameters of this system affect its radiation characteristics. Finally in section 4.6 we present a detailed calculation of the performance of a radial travelling-wave antenna of nearly-optimal dimensions and compare it with the wire-grid lens antenna.

4.2. Phase Centre of a Travelling-Wave Antenna

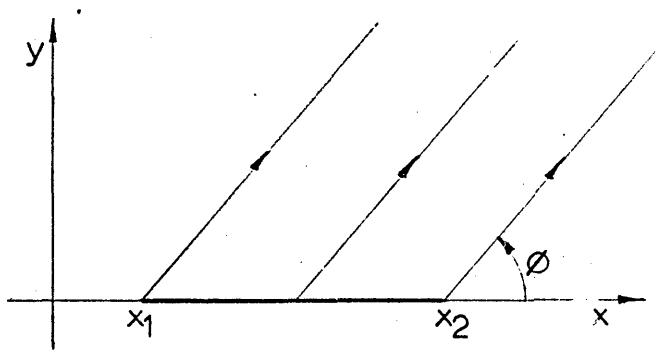

Fig. 4.1

Consider a travelling-wave antenna extending from x_1 to x_2 along the x axis (Fig.4.1). Denoting by $\exp\{-\gamma x\}$ the current distribution along the antenna, the far field in the horizontal plane is proportional to

$$E = \int_{x_1}^{x_2} e^{(-\gamma + jk_o\cos\phi)x}\, dx$$

$$= \frac{e^{(-\gamma + jk_o\cos\phi)x_1} - e^{(-\gamma + jk_o\cos\phi)x_2}}{-\gamma + jk_o\cos\phi} \qquad (1)$$

It is useful to transform this expression by writing

$$x_m = \frac{x_1+x_2}{2} \qquad x_1 = x_m - l/2 \qquad x_2 = x_m + l/2$$

Hence

$$E = \left[\frac{\sinh(-\gamma + jk_o\cos\phi)\,l/2}{-\gamma + jk_o\cos\phi}\right] e^{jk_o x_m \cos\phi}$$

where the factor $\exp\{-\gamma x_m\}$ has been omitted. The quantity in brackets is the radiation pattern of the antenna. It is approximately real for any value of ϕ providing the attenuation along the antenna is small (Real $\{\gamma\, l/2\} \ll 1$). In this case the phase of E is determined by the exponential factor which indicates that the antenna radiates as if it were a point source located at its mid-point. This is equivalent to saying that the antenna midpoint is the phase centre.

In the radial travelling-wave array the elements are relatively short and as a result the total attenuation along them is small. This means that the element midpoint can be regarded as the phase centre i.e. the effective radius of the array is equal to the distance from the element midpoint to the centre of the system.

However it is interesting to consider the case in which the total attenuation is large. (Real $\{\gamma\, l/2\} \gg 1$). Expression 1 reduces to

$$E \simeq \frac{e^{jk_o x_1 \cos\phi}}{-\gamma + jk_o\cos\phi} \qquad (1.a)$$

where the factor $\exp\{-\gamma x_1\}$ has been omitted. The phase variation of the denominator of expression 1.a is relatively small (less than

$\pi/2$) and thus we can say that the antenna phase-centre lies in the vicinity of the feed point. This suggests the possibility of an array of long Beverage elements fed from the outer ends. Such a system would be more expensive than the proposed one because of the need for buried cables connecting the centre of the system to the feed points in the periphery but it may give a higher directivity for the same size. We did not investigate this possibility.

4.3. General Beam Characteristics

In this section we shall examine how the beam characteristics depend on the parameters that define the geometrical configuration of the array. The following symbols are introduced:

M_b ..... number of driven elements per beam

δ ..... angular spacing between elements

r_a ..... distance from the element mid-points to the centre of the array (Fig.4.2)

r_2 ..... radius of the occupied area

l ..... element length

$g(\varphi,\theta)$ .... element radiation pattern

The field radiated by the beam pointing in the direction $\varphi=0$ is obtained by adding the contributions from the M_b driven element with the appropriate phase compensation. We have

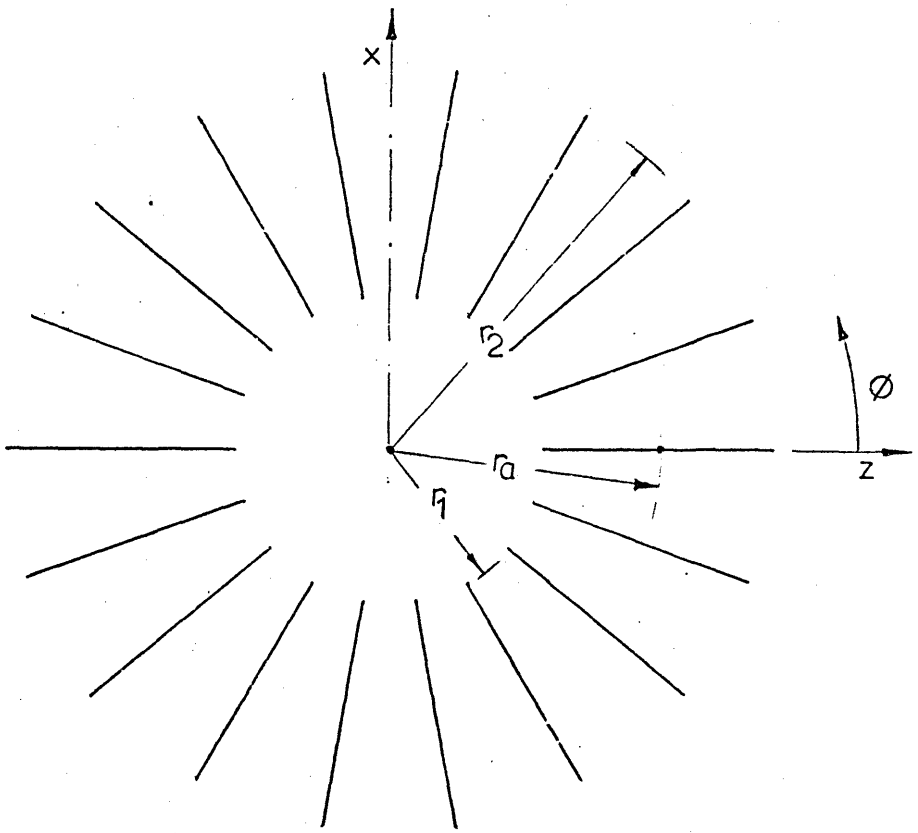

Fig. 4.2

$$E(\varnothing,\theta) = \frac{C}{r}\sum_{m=1}^{M_b} g(\varnothing-\varnothing_m,\theta)\exp\left\{jk_o r_a\left[\sin\epsilon\cos(\varnothing-\varnothing_m)-\cos\varnothing_m\right]\right\} \quad (2)$$

in which r is the distance from the observation point to the centre of the array and C is a factor that depends on the characteristics of the elements; $\varnothing_m$ defines the direction of element m and, for even M_b, is given by

$$\phi_m = (m-1)\delta - (M_b-1)\frac{\delta}{2} \qquad (3)$$

To study the directional characteristics of the system it is convenient to consider only the horizontal radiation pattern which is the most important. The attenuation along the elements and their interaction will be neglected (they are taken into account in later sections). Hence we have (See eq.2.8.a)

$$g(\phi - \phi_m \theta^0) = \frac{\sin X_m}{X_m} \cos(\phi - \phi_m) \qquad (4)$$

where

$$X_m = \pi \frac{l}{\lambda}\left[1-\cos(\phi - \phi_m)\right]$$

It follows that the horizontal radiation pattern is

$$E(\phi) = C \sum_{m=1}^{M_b} \frac{\sin X_m}{X_m} \cos(\phi - \phi_m) \exp\left\{jk_o r_a \left[\cos(\phi - \phi_m) - \cos\phi_m\right]\right\} \qquad (5)$$

where C is a normalisation constant. Expression 5 cannot be written in closed form but it can be easily evaluated on the digital computer for any value of the intervening variables.

A program of computations was carried out with a view to showing how the beamwidth and side-lobe ratio depend on the two main parameters of the array, the active sector angle and the ratio of element length to the radius of the antenna system r_2. The value chosen for the spacing between elements was five degrees which

ensures that for $r_2<15$ no grating lobes appear in the radiation pattern*.

In Figs. 4.3 and 4.4 the beamwidth is plotted against active-sector angle for several values of the ratio of element length to array radius (l/r_2= 0.2, 0.6, 0.8).

For a constant value of the active-sector angle the beamwidth increases with l/r_2. This is due to two reasons. Firstly, the effective array aperture is smaller for longer elements because the radius of the circumference defined by the phase centres decreases as l/r_2 increases

$$r_a = r_2(1-l/2r_2)$$

Secondly, reducing l widens the element radiation pattern which means that a wider sector contributes to the main lobe.

For constant l/r_2 the beamwidth decreases as the active-sector angle increases until this quantity reaches a value somewhat greater than the element beamwidth. This results from the fact that only the elements located within a sector whose angle is approximately equal to the element beamwidth can contribute effectively to the main lobe.

---

*A comparison of the radiation patterns for several values of the spacing and $r_2<15$ showed that up to 7.5° the grating lobes are negligible.

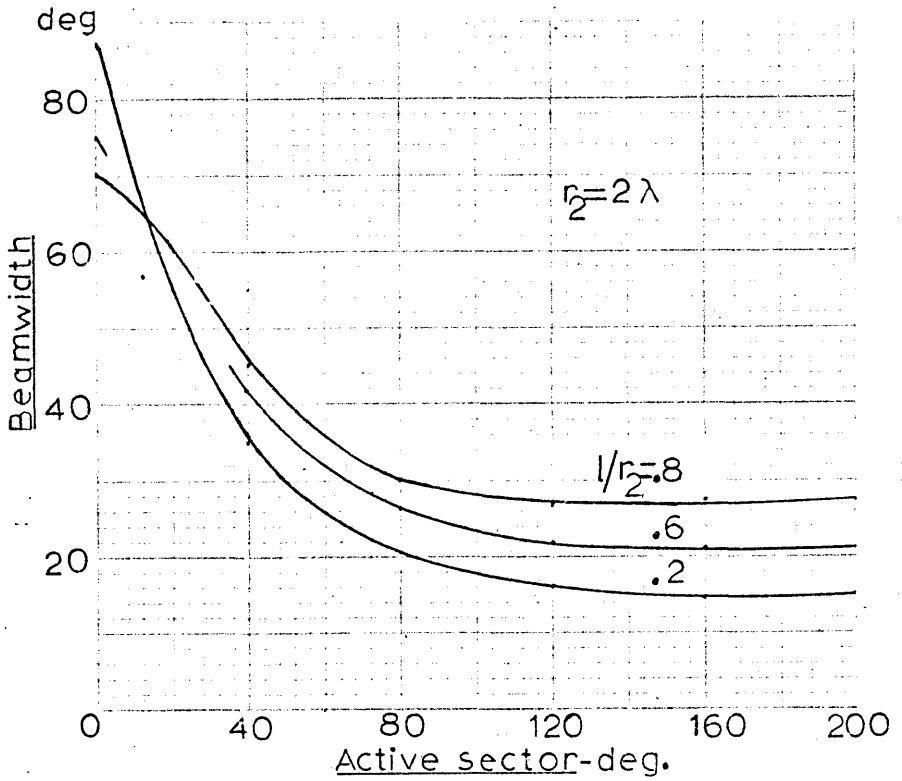
deg
80
60
40
20
0
Beamwidth
$r_2=2\lambda$
$l/r_2=.8$
.6
.2
40
80
120
160
200
Active sector-deg.

Fig. 4.3

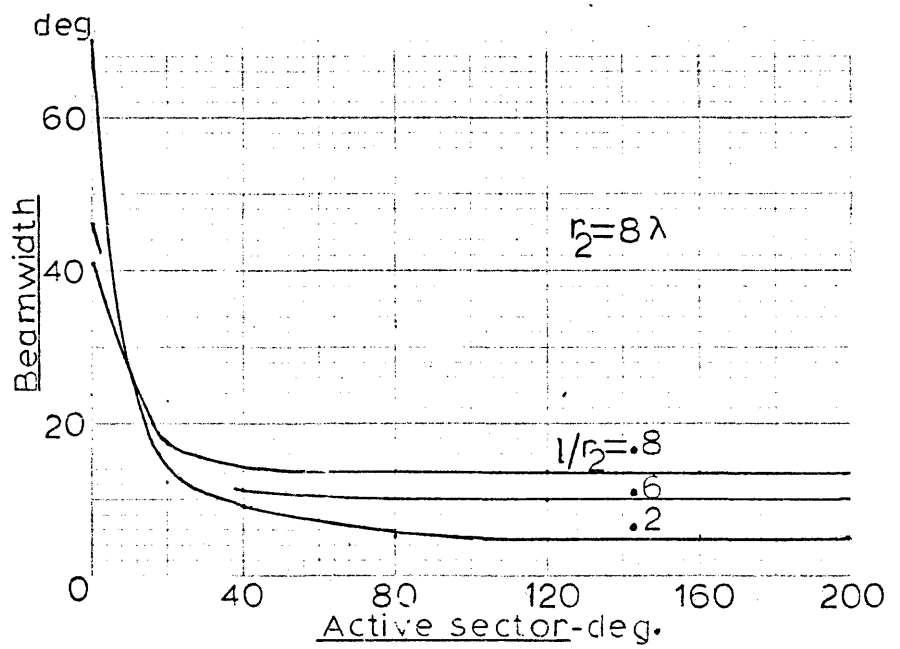
deg
60
40
20
0
Beamwidth
$r_2=8\lambda$
$l/r_2=.8$
.6
.2
40
80
120
160
200
Active sector-deg.

Fig. 4.4

In Figs.4.5 and 4.6 the side-lobe ratio is plotted against active-sector angle for values of the parameters of the system corresponding to those of Fig.4.3 and 4.4. The side-lobe level is generally better than that of the Beverage element. The curves exhibit maxima which are difficult to explain in physical terms. However, it is clear that the active sector must not exceed a certain value beyond which the side-lobe level increases rapidly, specially for long aerials. This is due to the fact that an element whose angular distance to the direction of maximum radiation is greater than about half its beamwidth, contributes mainly to the side lobes. To obtain a good side-lobe ratio the active-sector angle must not exceed about 130° at low frequency (array radius less then about 2λ) and must decrease with the frequency.

Fig.4.5 shows that for the same active sector the side-lobes increase with $1/r_2$. Comparing this with the previous conclusion regarding the dependence of the beamwidth on $1/r_2$, it is evident that in designing a practical system, a compromise between small size and low side-lobe level has to be reached.

Figs.4.7 and 4.8 illustrate how the beamwidth and side-lobe ratio vary with frequency. The curves for the beamwidth (Fig.4.7) exhibit two regions: a low frequency one where the beamwidth is approximately proportional to 1/f as for broadside arrays and a high frequency one where it varies slowly with frequency.

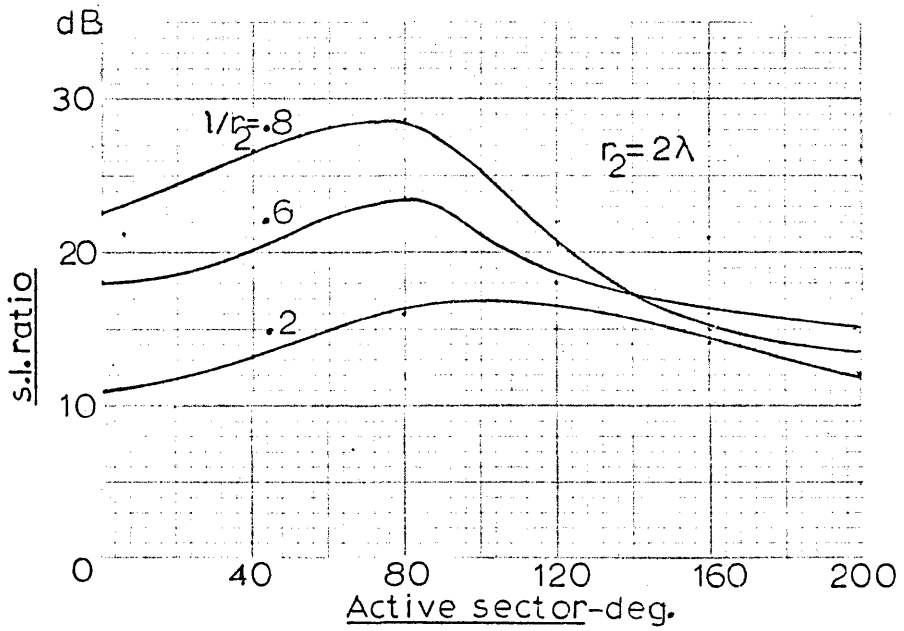
dB
30
20
10
0
s.l. ratio
1/r2=.8
.6
.2
r2= 2λ
40
80
120
160
200
Active sector-deg.

Fig. 4.5

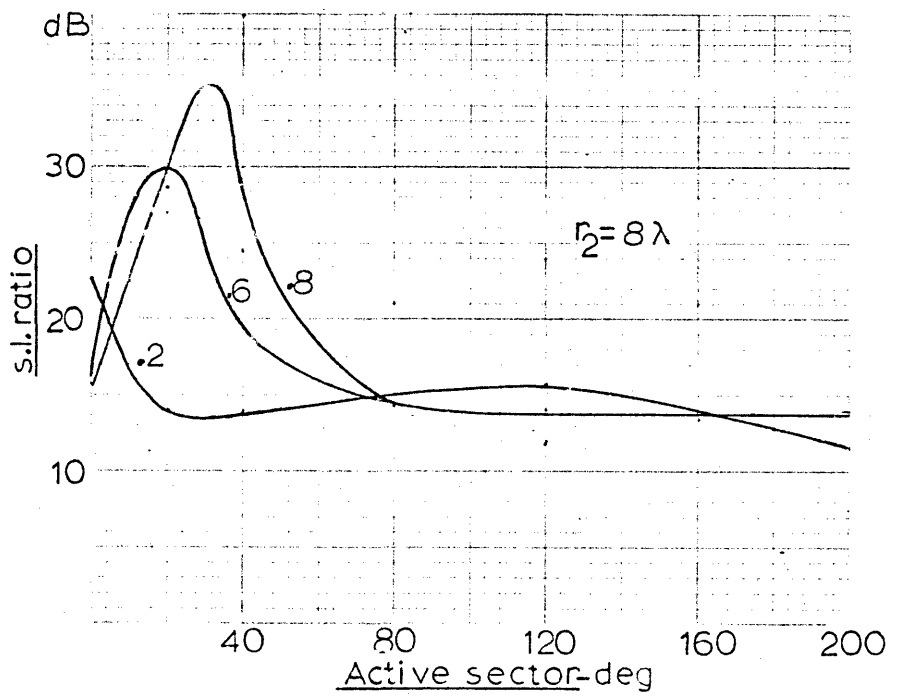
dB
30
20
10
s.l. ratio
r2= 8λ
.8
.6
.2
40
80
120
160
200
Active sector-deg

Fig.4.6

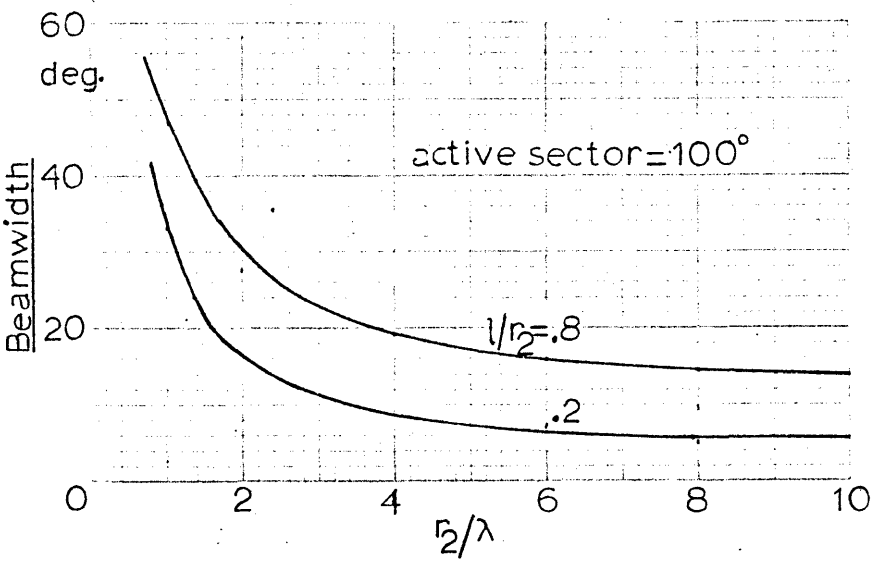
60
deg.
40
20
0
Beamwidth
active sector=100°
1/r2=.8
.2
2
4
6
8
10
r2/λ

Fig. 4.7

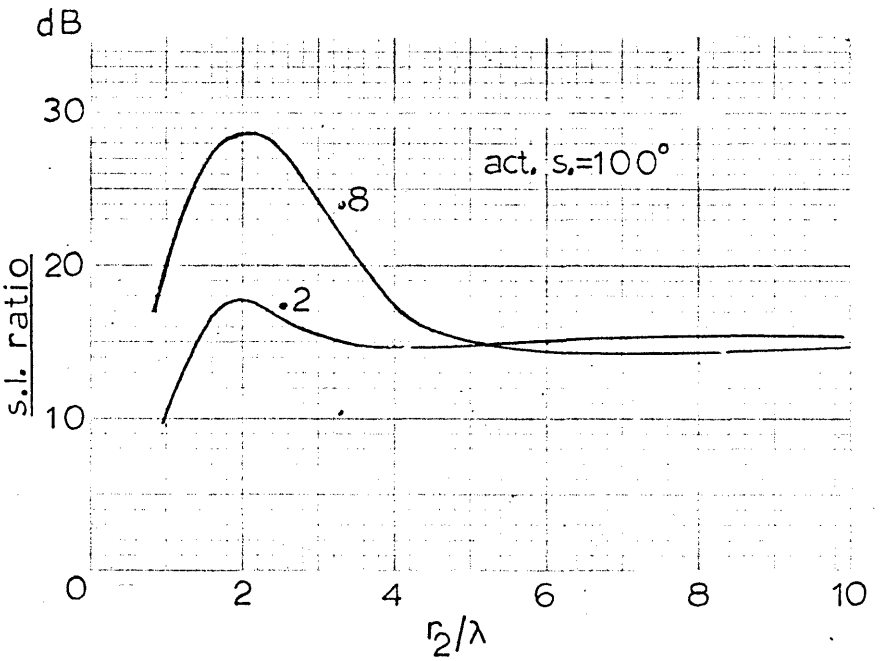
dB
30
20
10
0
s.l. ratio
act. s.=100°
.8
.2
2
4
6
8
10
r2/λ

Fig. 4.8

Fig. 4.7 shows again the existence of maxima in the side-lobe ratio.

In Figs. 4.9 and 4.10 the gain of the system relative to a diametral Beverage antenna is plotted against active-sector angle. The curves show the existence of broad maxima which occur for values of the active-sector angle somewhat greater than the element beamwidth. As it was to be expected the gain increases with $1/r_2$ but the difference between the curves is reduced as the frequency increases. This results from the fact that the optimum active sector narrows as the elements become longer in terms of wavelength.

We now summarise the preceding conclusions on the properties of the radial travelling-wave array.

(1) For the same occupied area the beamwidth increases with $1/r_2$.

(2) The active sector should not be greater than about 130° and should decrease with frequency.

(3) The side-lobe level is generally lower than that of a single Beverage antenna and therefore considerably better than that of a rhombic.

(4) The power gain is of the order of that of a diametral Beverage aerial and increases with $1/r_o$.

(5) The total beamwidth variation over a 10:1 frequency band ranges from 4:1 to 8:1 depending on $1/r_o$ and active sector.

(6) To obtain the best performance from a practical system it is

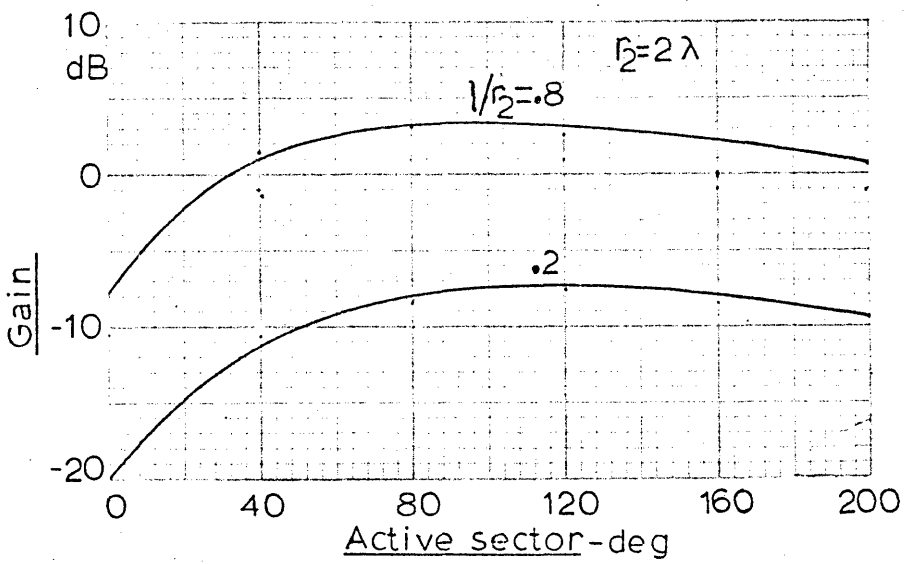

Fig. 4.9

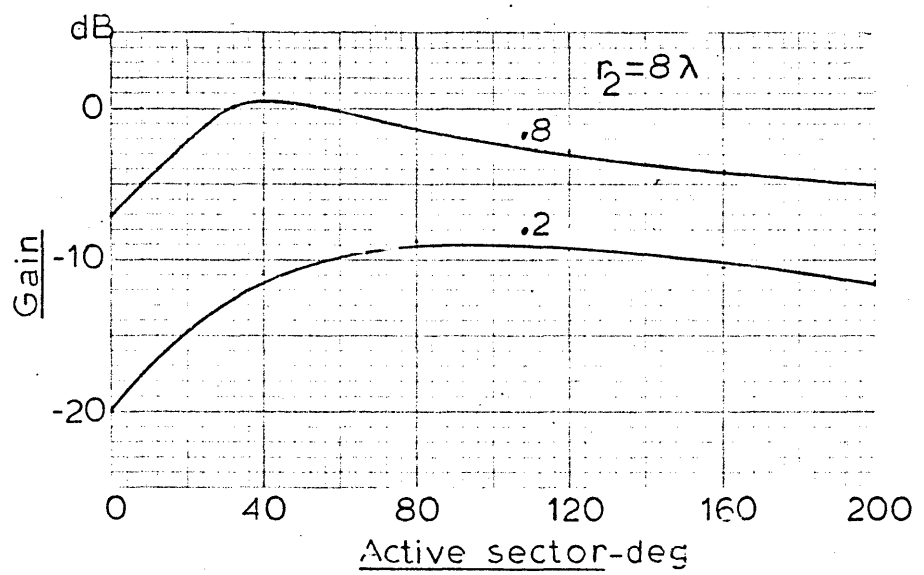

Fig. 4.10

convenient to reduce the active sector as frequency increases. It is suggested that an optimum array is one in which the active sector is somewhat greater than the element beamwidth.

(7) The radial travelling-wave antenna is a wide-band system in the sense that its radiation pattern exhibits low side lobes within a wide frequency band (of the order of 10:1) and the impedance of the array elements is approximately independent of the frequency.

4.4. Coupling Between Elements

The interaction between elements in an array causes their radiation patterns to be different from that of an isolated element. In the case of the radial travelling-wave antenna the fact that the coupling is not negligible does not have any serious consequences as long as back lobes remain low. A widening or narrowing of the element radiation pattern can be easily compensated by changing the ratio $1/r_2$.

In this section we attempt to correct the element radiation pattern by taking into account the field radiated by the currents induced on the other elements by the energised one.

It will be assumed that the spacing is 5° which, for $1/r_2=0.6$, implies that the distance between any two points on adjacent wires is much greater than their height. In this case the current on the coupled elements can be calculated by using a perturbation

method based on two assumptions

(a) the current on the active element remains approximately the the same as if it were isolated;

(b) the currents on the coupled elements can be calculated from the voltage induced on them by the energised one, using the equations valid for an isolated element.

Assumption (a) implies that the power transferred to the coupled elements is small. Assumption (b) implies that the propagation constant and the characteristic impedance can be considered to be the same as for an isolated element. It also means that the main contribution to the induced voltage is due to the active element. The validity of these assumptions will be examined at the end of the calculations in the light of the results obtained.

Let $E_m(\rho)$ be the electric field impressed on conductor m by the energised element located at $\varnothing=0$ (Fig.4.2). The voltage induced on a length $d\rho$ is $E_m(\rho)d\rho$. Assuming that the elements are matched this elementary voltage produces, at a point r, the current

$$di_m = - \frac{1}{2Z_c} E_m(\rho) \, e^{-\gamma_o |\rho - r|} \, d\rho$$

where γ_o and Z_c denote the propagation constant and the characteristic impedance of the elements. The current $i_m(r)$ is obtained

by integrating the above expression

$$-i_m(r) = \frac{1}{2Z_c} \int_{r_1}^{r_2} E_m(\rho) e^{-\gamma_o|\rho - r|} d\rho$$

$$= \frac{1}{2Z_c} \left\{ e^{-\gamma_o r} \int_{r_1}^{r} E_m(\rho) e^{\gamma_o \rho} d\rho + e^{\gamma_o r} \int_{r}^{r_2} E(\rho) e^{-\gamma \rho} d\rho \right\} \quad (6)$$

It is useful to write $E_m(\rho)$ in the form

$$E_m(\rho) = A_m(\rho)\, e^{-\gamma_m \rho} \quad (7)$$

where

$$\gamma_m = \gamma_o \cos \phi_m \quad (8)$$

Hence eq. 6 becomes

$$-i_m(r) = \frac{1}{2Z_c} \left\{ e^{-\gamma_o r} \int_{r_1}^{r} A_m e^{\gamma_o \rho C_m} d\rho + e^{\gamma_o r} \int_{r}^{r_2} A_m e^{-\gamma_o \rho C'_m} d\rho \right\} \quad (9)$$

where

$$C_m = 1 - \cos \phi_m$$

$$C'_m = 1 + \cos \phi_m$$

Obviously the most important contribution to the far field must come from the elements adjacent to the energised one. In this case ϕ_m is small and the first term in eq.9 is dominant (except for $r \simeq r_1$) since the integral in the second one contains a rapidly

varying exponential ($\gamma_o C'_n \simeq 2\gamma_o$). Consequently the dominant contribution to the far field of the induced currents comes from a forward travelling-wave and thus no significant deterioration of the element radiation pattern is likely to occur.

Expression 9 gives the current in the coupled element due to the voltages induced in the horizontal conductor. We must also take into account the voltages induced in the vertical terminations. These voltages lead to two waves travelling in opposite directions with propagation constant γ_o. Denoting the corresponding current by i_{vm} we have

$$i_{vm}(r) = -\frac{E_{1m}b}{2Z_c} e^{-\gamma_o r} + \frac{E_{2m}b}{2Z_c} e^{\gamma_o r} \qquad (10)$$

where E_{1m} and E_{2m} are the vertical components of the electric field at the inner and outer terminations of the coupled element. The sum of (10) and (9) gives the total current in the passive element.

To evaluate the integrals in eq.9 we need the expression for A_m. To this end E_m is split into components parallel and perpendicular to the energised element ($\varnothing = 0$).

$$E_m(\rho) = E_z(\rho) \cos \varnothing_m + E_x(\rho) \sin \varnothing_m \qquad (11)$$

Taking into consideration that, for the elements adjacent to the driven one, $\sin \varnothing_m \ll \cos \varnothing_m$ and that E_x is likely to be less than E_z we neglect the second term in (11) which greatly simplifies

the subsequent computations. Using the quasi-T.E.M. approximation we obtain from eqs.2.1 and 2.22 the following expression for E_z :

$$E_z = A_m = -j \frac{Z_o I}{2\pi k_o} \left\{ h_1^2 \ln \frac{\sqrt{x^2+4b^2}}{x} + 2\int_0^\infty \left[\frac{-jh_1^2}{-js+u_2} + \frac{\gamma_o^2}{k_o^2} \cdot \frac{(u_2+js)s}{-jn^2 s+u_2} \right] e^{-2bs} \cos xs \, ds \right\} \quad (12)$$

where

$$h_1^2 = k_o^2 + \gamma_o^2 \qquad u_2 = \sqrt{(n^2-1)k_o^2 - s^2}$$

$$Z_o = \sqrt{\mu_o / \epsilon_o} \qquad k_o = \omega \sqrt{\epsilon_o \mu_o}$$

$$x = \rho \sin \phi_m$$

and n is the refractive index of the ground.

Obviously the integrals in eqs.9 and 12 have to be evaluated numerically on the digital computer*. As indicated above, to obtain the total current eq.10 must be added to eq.9. To evaluate eq.10 it is accurate enough to calculate E_{1m} and E_{2m} by using the formulae for perfectly-conducting ground

$$E_v \simeq -\frac{Z_o I}{2\pi} \cdot \frac{2b}{x^2+4b^2} \quad (13)$$

---

* In later computations Simpson's rule with 20 points per wavelength is used.

where

$$x = \begin{cases} r_1 \sin \phi_m & \text{for} \quad E_v = E_{1m} \\ r_2 \sin \phi_m & \text{for} \quad E_v = E_{2m} \end{cases}$$

In Fig. 4.11 the amplitude and phase of the current in a coupled element adjacent to the driven one (calculated from eqs. 9, 10, 12 and 13) are plotted against **r**. The results refer to a radial travelling-wave antenna of typical dimensions:

$r_1 = 60m \quad r_2 = 150m \quad b = 1m \quad \epsilon_r = 15 \quad \sigma = 0.01$ S/m

and were calculated for a frequency near the centre of the h.f. band (f = 12 MHz).

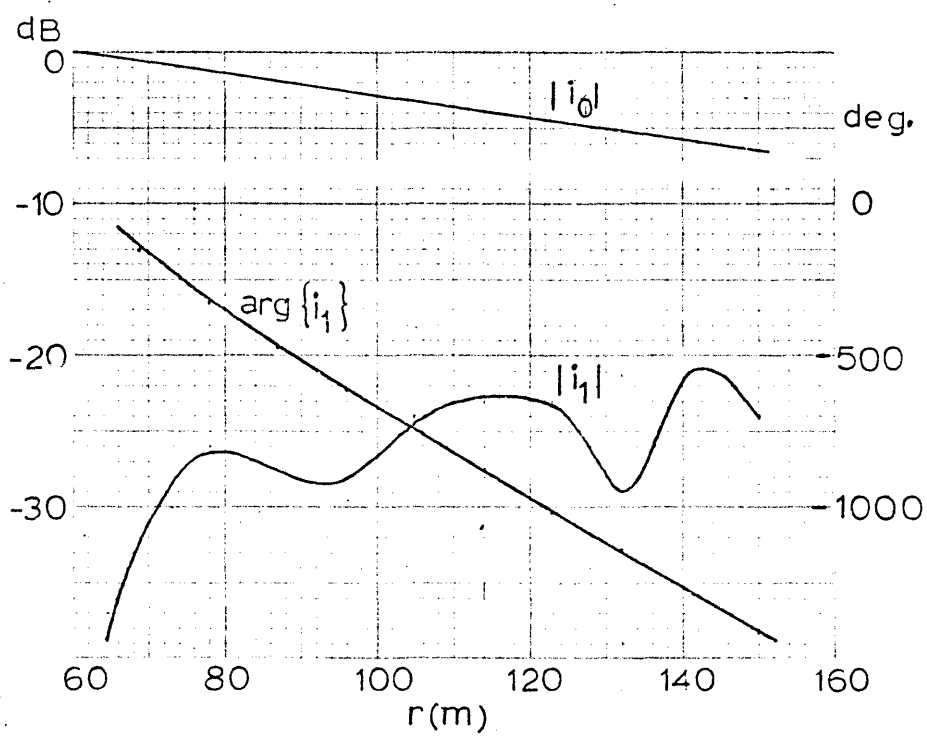

Fig. 4.11

Fig. 4.11 shows that:

(a) The current in the coupled element is lower than that in the driven element by at least 15 dB for almost the whole length of the elements.

(b) The phase of the induced current decreases almost linearly with r i.e. the dominant component in the current is an outward travelling wave. Hence no noticeable degradation of the element radiation pattern should result from the coupling.

Under the above-mentioned conditions the coupling can be ignored in the subsequent computations of the characteristics of the radial travelling-wave antenna.

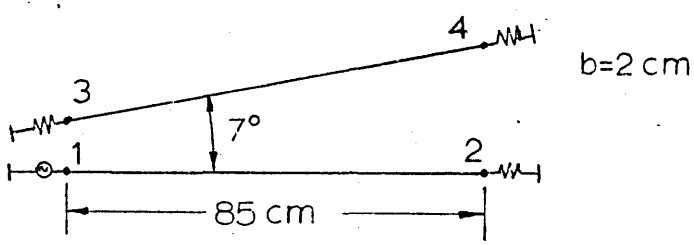

Fig. 4.12

The foregoing perturbation theory is based on the assumption that the power transferred from the driven element to the coupled ones is small. The results obtained in the example of Fig. 4.11 are consistent with this assumption, which gives confidance in the analysis. However, to assess its accuracy we have measured the

end currents for the system of two inclined wires shown in Fig.4.12. The results are condensed in Table III. They show a reasonably good agreement between theory and experiment for port 4 but a large deviation for port 3. This is thought to be mainly due to imperfect matching at terminals 3 and 4. From a practical point of view the fact that the results are reasonably accurate for port 4 is considered to be sufficient.

Table III

Coupling (dB)

	Experimental			Theoretical	
f(MHz)	2	3	4	3	4
400	0	-18	-12	-38	-13
500	0	-17	-12	-33	-13
600	0	-12	-11	-36	-13
700	0	-11	-10	-33	-13
800	0	-10	-10	-30	-14
900	0	-15	-12	-34	-14

4.5. Noise Factor

In this section we calculate the noise temperature of the radial travelling-wave antenna and examine the reason why wide-band amplifiers must be inserted between the Beverage elements and the power dividers in the beam-forming network (See Fig. 1.4).

It will be assumed that the external noise sources are uniformly distributed in the sky i.e. the received noise power does not depend on the directivity of the aerial. Thus, the external noise power at the receiver input can be written in the form

$$N_e = k(T_a - T_o)\, B/L_s \qquad (13)$$

where

k ..... Boltzmann constant

T_o ..... temperature of the system

T_a ..... equivalent antenna temperature (1)

B ..... receiver bandwidth

L_s ..... antenna loss

It is convenient to transform (13) by writing

$$L_s = L_a/G_N$$

in which L_a is the loss in the aerial system if no amplifiers or power dividers are present, (single beam system) and G_N is the gain of the combination amplifier-power divider. Hence

$$N_e = k\,(T_a - T_o)BG_N/L_a \qquad (14)$$

If F_T is the amplifier noise figure, the internal noise power at the output of the power dividers is[2]

$$N_i = kT_oBG_NF_T \qquad (15)$$

Since the noise at the output of the various power dividers is uncorrelated, the noise level at the receiver input will be equal to N_i. If the noise figure of the receiver is F_R we can define an equivalent input noise power which takes this into account

$$N_i = kT_oB\ (G_NF_T + F_R - 1) \qquad (16)$$

By adding (14) and (16) we obtain the total noise power at the receiver input

$$N_R = kT_oBG_N\ \left(\frac{T_a - T_o}{T_oL_a} + F_T + \frac{F_R - 1}{G_N}\right) \qquad (17)$$

Dividing by $k_oT_oB\ G_NL$ gives the noise figure of the aerial system

$$F_s = \frac{T_a}{T_o} - 1 + L_a\left(F_T + \frac{F_R - 1}{G_N}\right) \qquad (18)$$

In order to avoid an unnecessary degradation of the signal-to-noise ratio, the quantity T_a/T_oL_a must always be much greater than $F_T + (F_R-1)/G_N$. In the U.K. the lowest value of T_a/T_o in the frequency band 3-30 MHz is about 15 dB[1] and occurs at 30 MHz. At this frequency L_a is 9 dB (See Table IV, section 4.6). Assuming $F_T = F_R = G_N = 6$dB, the degradation of the signal-to-noise ratio due to the internal noise is

$$\frac{F_s}{T_a/T_o} \simeq \frac{31 + 8 \times (4+3/4)}{31} \simeq 2.2 <> 3.5 \text{ dB}$$

If the amplifiers are eliminated and each power divider provides 12 outlets*, we have

$$F_T = 1 \qquad G_N = 1/L_D = 1/12$$

where L_D is the loss in the power dividers. The degradation of the signal-to-noise ratio is now

$$\frac{31 + 8 \times (1+36)}{31} = 9.2 <> 9.6 \text{ dB}$$

Therefore, at times when the external noise level is very low and the interference from undesired signals negligible, the introduction of amplifiers in the beam-forming system may lead to an improvement of 6dB in signal-to-noise ratio at 30MHz. However, if the antenna is to operate in a site noisier than that assumed above, the utilisation of wide-band amplifiers may bring no benefit.

4.6. Performance of the Proposed System

In section 4.3 we analysed the beam characteristics of

---

* It is assumed that only 12 receivers are connected simultaneously to the aerial system and that the phasing networks are associated with the receivers in which case only the beams being used are synthesised.

the array of radial travelling-wave antennas and showed how these characteristics depend on the geometrical configuration of the array. In this section we define a proposal for a practical receiving aerial system, to operate in the frequency band 3-30 MHz, and examine in detail its theoretical performance.

As indicated in 4.3. the main characteristics of the radial travelling-wave antenna are largely determined by three parameters: radius of the occupied circle (r_2), ratio of element length to radius (l/r_2) and active-sector angle. As the optimum value of the active sector depends on the length of the elements only two parameters have to be chosen independently.

It does not appear to be easy to define quantitatively an optimum antenna so that an optimisation technique could be used to determine the values of those parameters. The fact that increasing l/r_2 reduces the directivity but increases the absolute gain implies that the choice of this parameter has to be based on a compromise between directivity and gain. A value of l/r_2 equal to 0.6 is proposed.

For a beamwidth of 10 degrees at 24 MHz the array radius r_2 must be approximately 150m, i.e. the element length will be 90m. This is about 1/3 the length of the antenna considered in section 3.6 and thus its gain will be approximately 10 dB lower. However this difference is compensated by the array gain as shown by the

analysis of section 4.3. where the gain of the radial travelling-wave antenna was compared with that of an element one diameter long.

As indicated in section 3.8, to avoid a degradation of the radiation pattern of the Beverage aerial due to the field from the terminal wires, the ratio of length to height must be of the order of a hundred. An element height of 1m seems therefore adequate.

The outputs of the elements are combined in hybrid transformers (See Fig.1.4) which means that the number of active elements per beam is restricted to the integer powers of 2. We propose to divide the frequency range 3-30 MHz into three bands; 32 elements (active sector=160°) are used from 3 to 6 MHz, 16 elements (80°) from 6 to 18 MHz and 8 elements (40°) from 18 to 30 MHz. These frequency bands were obtained by trial and error and are not necessarily optimum.

In detail the characteristics of the proposed antenna system are:

radius of the occupied circle		150m
element length		90m
" height		1m
" spacing		5°
Number of elements per beam	3-6 MHz	32
	6-18 MHz	16
	18-30 MHz	8

Number of hybrids per beam		15
Number of delay lines per beam		7
Ground constant used in the calculations	dielectric constant	15
	conductivity	0.01s/m

The radiation characteristics of this system were calculated on the digital computer for six values of the frequency: 3, 6, 12, 18, 24, and 30 MHz*. The program was divided into several subroutines to calculate successively the following quantities:

(1) Characteristic impedance of the Beverage aerials; attenuation and phase velocity of the current wave.

(2) Reflection coefficients for horizontal and vertical polarisations.

(3) Field radiated by an isolated Beverage element taking into account the field due to the vertical end wires and the attenuation of the current wave.

(4) Field radiated by the array calculated by superposition of the fields of the active elements after phase correction (See expression 2).

(5) Directivity calculated by integrating the results (4) over a sphere. Power gain. Radiation patterns in the principal

---

* The time required for these calculations is 8 minutes on the IBM 7094 computer.

Table IV

Radiation Characteristics of the

Radial Travelling-Wave Antenna

				Horizontal Pattern		Vertical Pattern 3 dB points	
Freq. MHz	Active sector	Gain dB	Directivity dB	Beamwidth deg.	S.l.ratio dB	Upper deg.	Lower deg.
3	160°	-2	13	29	14	59	9
5		2	16	19	16	39	7
6		4	18	22	17	39	7
12	80°	7	19	13	16	27	6
18		9	19	11	14	22	5
18		11	20	13	18	20	5
24	40°	12	21	11	16	20	5
30		13	22	9	15	18	5

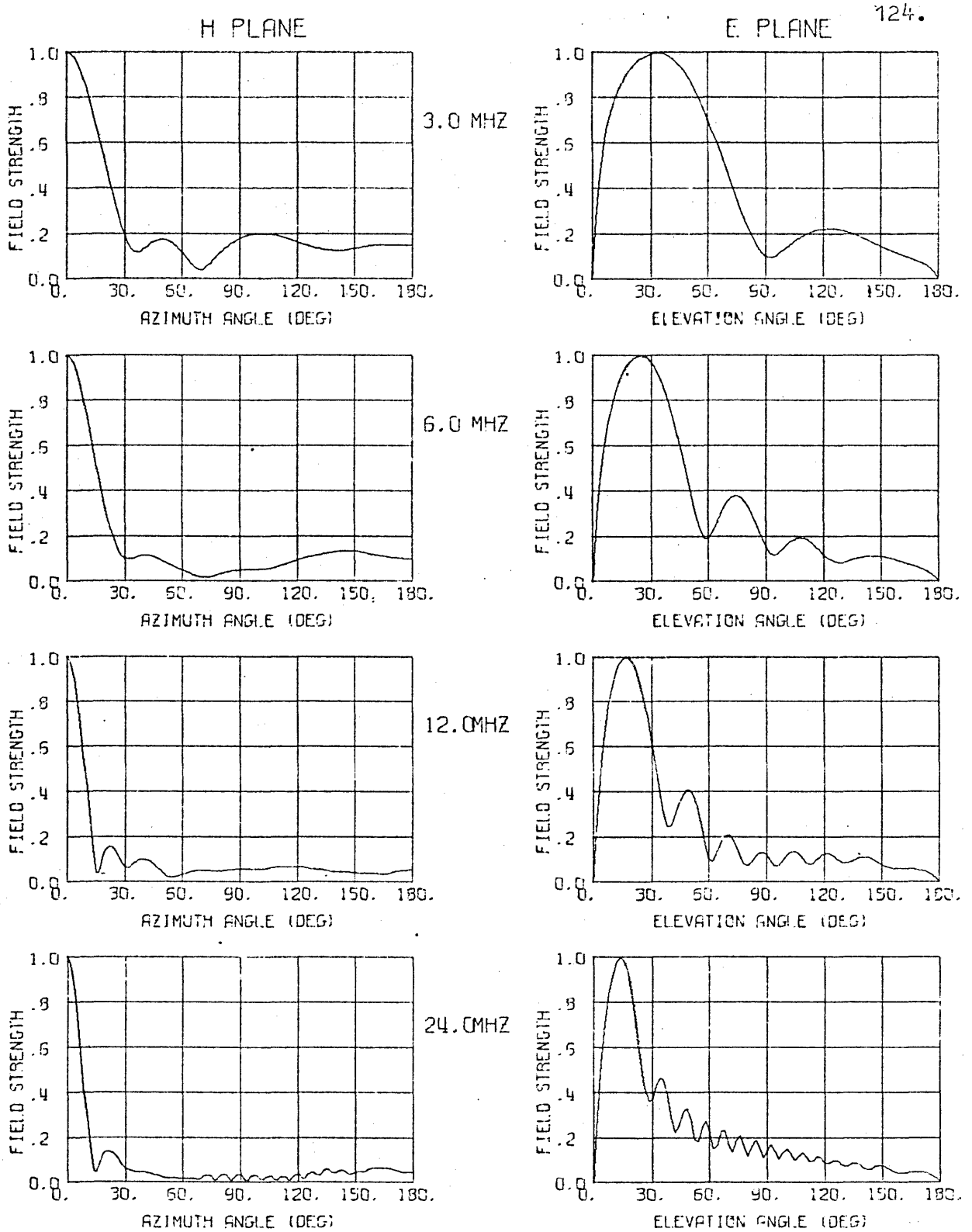

RADIATION PATTERNS OF RADIAL T.W. AERIAL (RADIUS= 150M)

Fig. 4.13

planes.

(6) Beamwidth and side-lobe ratio for the patterns obtained in (5). The program includes also a subroutine to plot the radiation patterns shown in Fig. 1.13. The remaining results are condensed in Table IV.

An examination of these results shows that

(a) The radial travelling-wave antenna is capable of covering the whole high-frequency band with good side-lobe performance (side-lobe ratio greater than 14 dB).

(b) The gain and directivity are comparable to those of a Beverage antenna one diameter long (See Table II, ch.2) but its main beam is narrower in the horizontal plane and broader in the vertical plane. This is the advantage that it has over the arrangement of diametral Beverage antennas mentioned in section 1.2.

*

* *

In Figs. 4.14 to 4.16 the performance of the radial travelling-wave antenna is compared with that of the Luneberg lens as given in ref.3. Figs.4.14 and 4.15 show that the proposed system exhibits slightly broader beams, but lower side-lobe level, than the Luneberg lens antenna. The difference in side-lobe level is significant at the lower frequencies (6 dB at 6MHz).

The directivity and power gain of the two systems are plotted in Fig. 4.16. The Luneberg lens has a higher directivity, but the difference between the two systems is small (less than 2 dB). The gain of the proposed antenna is lower but this is of little practical importance for the reasons discussed in section 3.5.1 i.e. because of the high external noise level in the 3-30 MHz band.

Thus it appears that the proposed system has a performance comparable tc the Luneberg lens antenna. However, its constructional simplicity is a considerable advantage over the lens antenna.

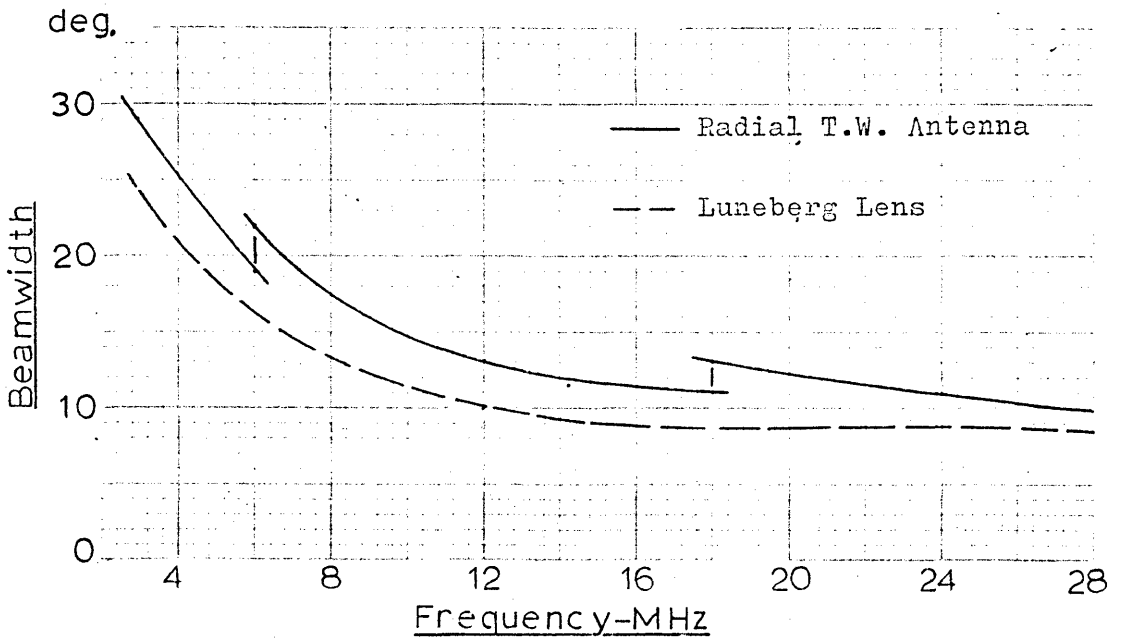

Fig. 4.14

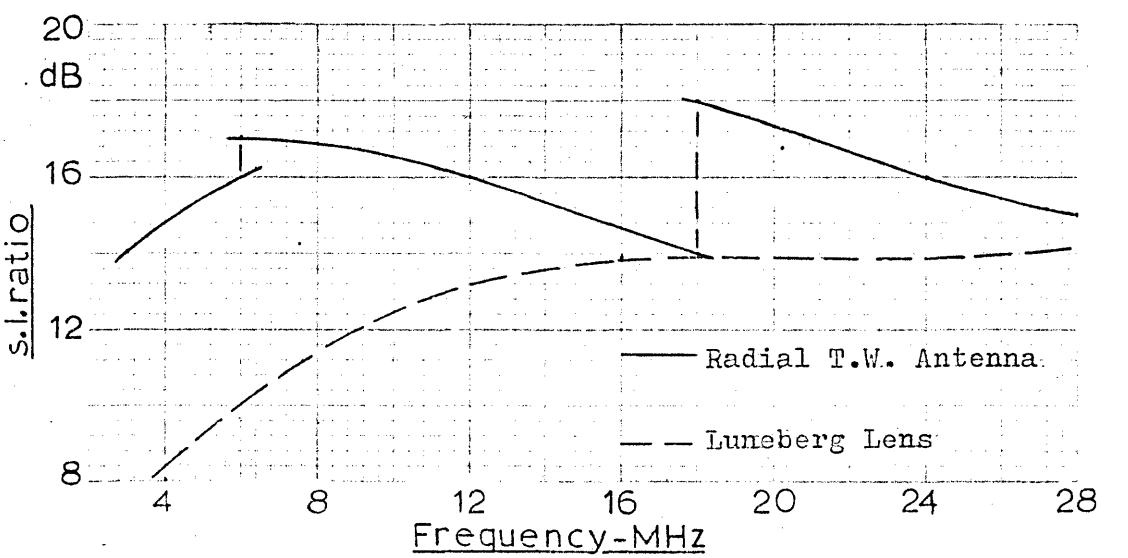

Fig. 4.15

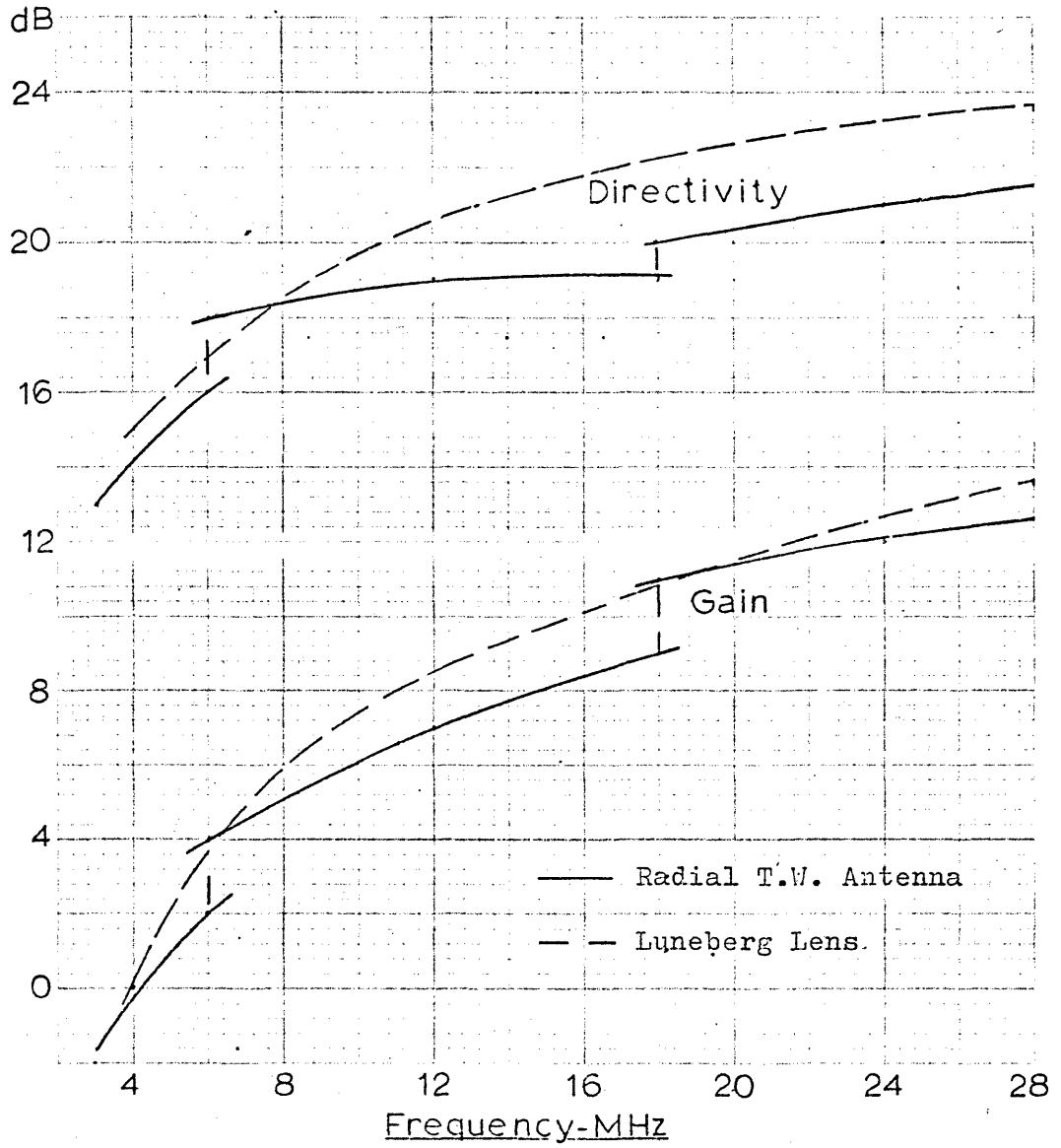
dB
24
20
16
12
8
4
0
Directivity
Gain
Radial T.W. Antenna
Luneberg Lens.
4
8
12
16
20
24
28
Frequency-MHz

Fig. 4.16

References

1. "World distribution and characteristics of atmospheric radio noise" C.C.I.R. report n°322, Geneva 1963.

2. M.Schwartz "Information transmission, modulation, and noise" McGraw-Hill 1959, section 5.9.

3. E.Jones, R.Tanner, E.Sharp, M.Andreason and F.Harris "Performance of the wire-grid lens h.f. antenna" I.R.E. Trans. on Antennas and Propagation vol. AP-15 p. 744, November 1967.